Emanuel Abreu Antunes Carlos

Licenciado em Ciências de Engenharia
de Micro e Nanotecnologias

Oxide transistors produced by solution: Influence of annealing parameters on properties of the insulator

Dissertação para obtenção do Grau de Mestre em
Engenharia de Micro e Nanotecnologias

Orientadora: Doutora Rita Maria Mourão Salazar Branquinho,
Prof. Auxiliar, FCT-UNL
Co-orientadora: Doutora Elvira Maria Correia Fortunato,
Prof. Catedrática, FCT-UNL

Júri:

Presidente: Doutor Rodrigo Ferrão Paiva Martins,
Prof. Catedrático, FCT-UNL
Arguente: Doutor Luís Miguel Nunes Pereira,
Prof. Auxiliar, FCT-UNL
Vogal: Doutora Rita Maria Mourão Salazar Branquinho,
Prof. Auxiliar, FCT-UNL

FACULDADE DE CIÊNCIAS E TECNOLOGIA
UNIVERSIDADE NOVA DE LISBOA

Dezembro 2015

Oxide transistors produced by solution: Influence of annealing parameters on properties of the insulator

Faculdade de Ciências e Tecnologia

Universidade Nova de Lisboa

Acknowledgements

First I would like to thank my institution, the Faculty of Science and Technology of the Universidade NOVA de Lisboa, and my department, Materials Science, for all the experiences provided over these years with a great academic life.

Secondly, I would like to send my greatest gratitude to Professor Rodrigo Martins and Professor Elvira Fortunato for their dedication and hard work in creating the course of Micro and Nanotechnology and also for the great conditions and infrastructures that they offer in CENIMAT| I3N and CEMOP to investigate in several areas allowing the realization of my thesis.

To my supervisors Rita Branquinho and Elvira Fortunato with whom I had the privilege of working, who supported me along the way in what I needed and were always open-minded to new ideas. I also would like to thank the remaining members of the group, including Pedro Barquinha, Joana Pinto, Ana Santa, Daniela Salgueiro, Asal Kiazadeh, Daniela Gomes, Jonas Deuermeier, Cristina Fernandes, Diogo Lima, Marta Ferreira, Ganga Bahubalindruni, Jorge Martins, Ana Rovisco and Allegra Sacchetti by the brainstorming in the meetings helping to clarify my doubts. A special thanks to Rita Branquinho for her extensive help being always ready to help even when she had a lot of work.

To Alexandra Gonçalves and Carolina Marques for providing me everything I needed and to Tomás Calmeiro for obtaining the AFM images of my samples. In order to not forget anybody I express my deepest gratitude to the rest of this institute for always being present to support me with tasks reaching from work related technical support.

To all my course mates of Micro and Nanotechnology that accompanied me throughout the degree. To my closest friends during all my studies: Diogo Lima, Luis, Trofas, Farah, Tiago, Catarina, Raquel, Susana, Ana, Diogo Vaz, Júlio, Bruno, Inês, Paul and Rodrigo. What a great time we had together. The fun, the jokes, the parties, the good and the bad, those memories will always accompany me.

To the junior enterprise iNOVAfuture for the challenges raised and stimulation of new ideas.

I would like to thank my loved ones, starting with my family, who have supported me throughout the entire process for putting up with me and for making me the man I am today. To my grandparents and parents, for their incredible support, for being outstandingly comprehensive, for their motivation, and for their help. Without them, none of this would be possible.

To my sister and brother, Joana and Ludgero, for their help, even when they did not knew they were helping.

To my girlfriend and best friend, Sara Serrano, for her presence and comprehension keeping me happy, peaceful and sane.

To my comrades firefighters by the good moments spent and lived experiences.

Abstract

Solution processing of amorphous metal oxides has been lately used as an option to implement in flexible electronics allowing to reduce the associated costs and get a better performance. However the research has focused more on semiconductor layer instead of focusing on the insulator layer that is related to the stability and performance of the devices. This work aims to evaluate amorphous aluminum oxide thin films produced using different precursor solutions and processing synthesis, and the influence of different annealing parameters on properties of the insulator layer in thin film transistors (TFTs) using different semiconductors. Optimized dielectric layer was obtained for aluminum nitrate based precursor solution using urea as fuel with 0.1 M concentration for an annealing of 30 min assisted by far ultraviolet (FUV) irradiation at a lamp distance of 5 cm. These thin films were applied in gallium−indium–zinc oxide (GIZO) TFTs as dielectric showing the best results for TFTs annealed at 180 ^{o}C with FUV irradiation: a good reproducibility with an average mobility of 17.32 ± 4.15 cm^2 V^{-1} s^{-1}, a subthreshold slope of 0.11 ± 0.01 V dec^{-1} and a turn-on voltage of - 0.12 ± 0.06 V; a low operating voltage and a good stability over 9 weeks. Finally the dielectric layer was applied in solution processed indium oxide (In_2O_3) TFTs at low temperatures and in flexible substrates for GIZO/AlO_x TFTs annealed at 200 ^{o}C with FUV irradiation. The obtained results are equivalent to the published ones and in some cases surpassing the actual state of the art.

Keywords: Aluminum oxide, combustion reaction, FUV irradiation, low temperature, solution TFTs, low operating voltage

Resumo

O processamento por solução de óxidos de metal amorfos tem sido usados como opção para implementar em eletrónica flexível permitindo reduzir os custos associados e obter um melhor desempenho. No entanto a investigação tem-se focado mais na camada do semicondutor e não tanto na camada isolante que está relacionada com a estabilidade e desempenho dos dispositivos. Este trabalho tem como objetivo avaliar filmes finos amorfos de óxido de alumínio produzidos usando diferentes soluções precursoras e sínteses de processamento, assim como a influência de diferentes parâmetros de recozimento nas propriedades do isolante em transístores de filme fino (TFTs) utilizando diferentes semicondutores. A camada dielétrica otimizada foi obtida para a solução precursora baseada em nitrato de alumínio usando ureia como combustível com uma concentração de 0,1 M para um recozimento de 30 min assistida pela irradiação *Far UltraViolet* (FUV) para uma distância da lâmpada de 5 cm. Estes filmes finos foram aplicados em TFTs de óxido de gálio – índio – zinco (GIZO) como dielétrico apresentando os melhores resultados para os TFTs recozidos a 180 ºC com irradiação FUV: uma boa reprodutibilidade com uma mobilidade média de 17,32 ± 4,15 $cm^2 V^{-1} s^{-1}$, um *subthreshold slope* de 0,11 ± 0,01 V dec^{-1}e uma tensão de abertura de - 0,12 ± 0,06 V; uma baixa tensão de funcionamento e uma boa estabilidade ao longo de 9 semanas. Por fim aplicou-se a camada dielétrica nos TFTs de óxido de índio (In_2O_3) processado por solução a baixas temperaturas e em substratos flexíveis para TFTs de GIZO/AlO_x recozidos a 200 ºC com irradiação FUV. Os resultados obtidos são equivalentes aos publicados internacionalmente e em alguns casos superam o atual estado da arte.

Palavras-chave: Óxido de alumínio, reação de combustão, irradiação FUV, baixa temperatura, TFTs por solução, baixa tensão de funcionamento

List of Abbreviations

2-ME – 2-methoxyethanol

AFM – Atomic Force Microscopy

AMOLED – Active-Matrix Organic Light-Emitting Diodes

ATR – Attenuated total reflectance

CA – Citric Acid

CEMOP – Center of Excellence in Microelectronics and Optoelectronics Processes

CENIMAT – Centro de investigação de materiais

Cf – Capacity-frequency

CV – Capacity-voltage

DC – Direct current

DSC – Differential scanning calorimetry

DUV – Deep Ultraviolet

FIB – Focused ion beam

FTIR – Fourier Transform Infrared Spectroscopy

FUV – Far Ultraviolet

GIZO – Gallium Indium Zinc Oxide

IV – Current-voltage

LCDs – Liquid crystal displays

MIS – Metal-Insulator-Semiconductor

M-O-M – Metal oxide metal

MOSFET – Metal Oxide Semiconductor Field Effect Transistor

NA – Ammonium nitrate

NBS – Negative Bias Stress

OLED – Organic light-emitting diode

OV – Oxidizing valence

PBS – Positive Bias Stress

PET – Polyethylene terephthalate

PVD – Physical vapor deposition

R2R – Roll-to-roll

Rms – Surface roughness (Root mean square)

rpm – Rotations per minute

RV – Reducing valence

SCS – Solution combustion synthesis

SE – Spectroscopic Ellipsometry

SEM – Scanning Electron Microscope

SN – Silver nitrate

TFTs – Thin Film Transistors

TG – Thermogravimetry

U – Urea

UV – Ultraviolet

Vis – Visible

XRD – X-ray Diffraction

ZTO – Zinc Tin Oxide

List of Symbols

A – Area

c – Concentration

C_{ox} – Oxide capacity

C_D – Semiconductor depletion capacity

C_t – Total capacity

d – Thickness of the insulator

ε_0 – Permittivity of free space (8.854×10^{-12} F m^{-1})

F – Farad

g_m – Transconductance

h – Hour

Hz – Hertz

I_{DS} – Current between source and drain

I_G – Gate leakage current

I_{off} – Drain current in the off state

I_{on} – Drain current in the on state

J – Density of leakage current

k – Dielectric constant of the insulating material

L – Channel length

M – Molar concentration

min – Minute

^oC – Degrees Celsius

q – Charge

s – Second

S – Subthreshold slope

V_{DS} – Voltage between source and drain

V_{GS} – Voltage between source and gate

V_{Hyst} – Hysteresis

V_{on} – Turn-on voltage

V_T – Threshold voltage

W – Channel Width

ΔE – Conduction band offset

ΔS – Subthreshold slope variation

ΔV_T – Threshold voltage shift

Ω – Ohm

Table of Contents

List of Figures

List of Tables

Motivation and Objectives

Printed electronics is an area of research in great expansion due to potential applications in technology and their impact today in society. Consequently, the development of materials with applications in flexible electronics that can be processed by solution is of extreme importance, so solution-processed metal oxide thin-film transistors (TFTs) have been widely studied. In order to ensure a good viability, TFTs must have a good performance, reproducibility, low cost, reliability associated to a low temperature processing method to be compatible with low cost flexible substrates. The small size of transistors leads to technological problems in the semiconductor industry, however the performance of TFTs is also dependent of dielectric layer because the insulating layer between the gate electrode and the semiconductor contributes greatly to the electrical performance and stability of the devices. Taking this into account, the dielectric layer produced by solution will be studied in this master thesis.

The main objective is to produce, study and optimize thin films of aluminum oxide (Al_2O_3) by solution and apply these in electronic devices to determine which are the effects of annealing process on the overall performance. This will involve several tasks to evaluate the dielectric layer:

- Production and characterization of different precursor solutions;
- Production and characterization of MIS (Metal-Insulator-Semiconductor) structures using different solutions and temperatures;
- Influence of combination of ultraviolet (UV) irradiation with annealing in thin films properties.

Another goal is to implement the insulator in TFTs with several semiconductor oxides and characterize them, one produced by solution process (ZTO) and another by sputtering (GIZO), developed by the research group of CENIMAT in silicon substrates at 350 ºC. The optimized precursor solution of alumina and semiconductor will be used to produce TFTs at low temperatures.

Finally TFTs all processed by solution using a semiconductor reported in the literature will be produced and characterized.

1. Introduction

Nowadays silicon-based materials have been less used due to the necessity for emerging applications in electronics such as transparent flexible displays, flexible solar cells and large area applications because they do not show optical transparency. Organic materials have other problems like low carrier mobility and environmental issues. [1], [2] Solution-processed amorphous metal oxides can solve those problems, as well as demonstrate exceptional large-area uniformity, high dielectric constants and no need for vacuum processing conditions. Their solution processability have released new possibilities for low cost printable, as roll to roll (R2R), and transparent devices using flexible substrates.[1]–[4] Typically spin-coating, inkjet-printing, dip-coating and spray-coating are the main options to solution process oxide semiconductors and gate dielectrics.[3], [5]

1.1 High-k dielectrics

By going to a small size scale of the field effect transistor in integrated circuits, the thickness of SiO_2 has to go to the nanometer scale, but the leakage current of SiO_2 is affected, due to the appearance of tunneling effects.[6]–[10] Therefore researchers took measures to solve the problem by finding ultrathin dielectrics with high-k dielectric, high capacitances, low leakage current densities, smooth surfaces and high thermal stability.[11]–[13] The combination of these characteristics allows to induce large charge densities in the semiconductor and assure low voltage operations.[9, 14] Some of the most studied inorganic dielectrics are aluminum oxide (Al_2O_3), hafnium oxide (HfO_2), tantalum oxide (Ta_2O_5), zirconium oxide (ZrO_2) and their mixtures.[15], [16]

Amongst many potential materials (Figure 1.1), Al_2O_3 is a desirable gate insulator because of its characteristic properties such as high dielectric constant (~9) combined with large band gap (8.9 eV), low interfacial trap density with semiconductors, compatibility at low temperatures, high breakdown electric field (4 – 5 MV/cm) and remains amorphous after typical processing conditions. Also it is an amphoteric oxide and has a quite high thermal conductivity (30 $Wm^{-1}K^{-1}$). [7], [17]–[19]

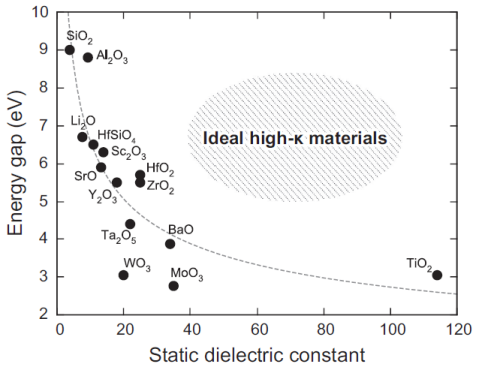

Figure 1.1 – Relation between the energy gap and the static dielectric constant for different materials considered as high-k dielectrics.[20]

1.2 High performance TFTs at low temperatures

In the last years, amorphous metal oxides produced by solution can be compared with oxide semiconductor films developed by physical vapor deposition (PVD), but usually it is necessary an extra annealing process at high temperatures to induce a condensed and uniform film, which is not compatible with flexible low cost substrates.[21]–[24]

In order to solve the above problem, researchers tried a new strategy to reduce the temperature needed for the production of solution-processed metal oxide TFTs by using self-energy generating combustion chemistry.[1] The process of solution combustion synthesis (SCS)

allows to reach the energy-efficient synthesis of bulk materials such as carbides, III-V semiconductors, metal oxides, refractory nitrides and intermetallic compounds.[25]–[27] One of the advantages of using the SCS method is that there is no need of any special equipment to provide the additional heat, due to the combustive reaction of the precursor compounds which produces self-sustaining heat and supplies sufficient energy to decompose all matter to form the metal oxide (Figure 1.2). Typically the solution of the redox system is constituted by an oxidizer, normally nitrates of metal precursor and a fuel like acetylacetone, urea or citric acid.[1], [27]–[29]

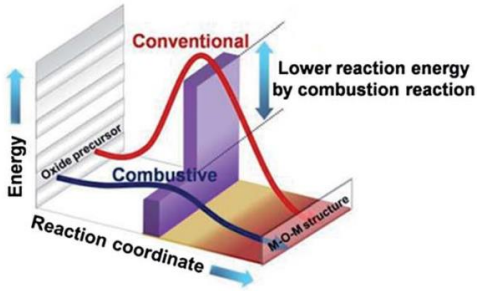

Figure 1.2 – Comparison of the energy required for a conventional reaction relatively to a combustion one.[6]

Another way to get good viability of the devices and integrated circuits at low temperatures, is combining deep-ultraviolet (DUV) treatment with thermal annealing in order to have an improved condensation and film densification in amorphous metal-oxide semiconductors.[2] The solution based amorphous metal oxides thin films require DUV treatment (UV lamp main peaks at 184.9 nm (10%) and 253.7 nm (90%)) to remove a substantial amount of residual organic components. The exposure to high energy photons induces a cleavage of alkoxy groups, active metals and oxygen atoms to simplify M-O-M network formation. The UV irradiation can break the polymeric chains into smaller fragments in less than 10 min which induces a rapid degradation, removal of oxygen and carbon that promotes the densification of the film.[2], [30]–[34]

Recently a group of researchers used a shorter UV wavelength (160 nm) combined with thermal annealing at low temperatures that accelerates the condensation process resulting in a rapid formation of a continuous M-O-M structure in the In_2O_3 film. Furthermore this allowed a reduction of process time making it more compatible with R2R process.[35]

1.3 Metal-Insulator-Semiconductor capacitors

Capacitors are part of electronic circuits used to store electric power by accumulating internally unbalanced levels of electrical charges. This electric component can have various sizes and shapes but the typical structure consists of two conductors, named plates, which transport equal but opposites charges (-q and +q) and the insulator, with a fixed thickness (*d*), used to separate the conductive plates.[36] The charge is given by the potential difference (V) between the plates and by the capacity (C); q = CV.

Faraday defined that the capacity, measured in Farads, of any capacitor with parallel-plates depends of the plates area (A), the thickness of the dielectric (*d*), the dielectric constant of the insulating material (κ) and vacuum permittivity (ε_0). Therefore C depends on the size and geometry of the plates but does not depend on the charge or the potential difference. [37]

$$C = \kappa\varepsilon_0 \frac{A}{d} \tag{1.1}$$

For the Metal-Insulator-Semiconductor (MIS) capacitors case, the capacity value changes with the applied voltage due to the presence of a semiconductor like silicon. To determine the capacity value in MIS capacitors, the characterization is done with the capacity-voltage (CV) curves and involves the application of a biased voltage at the capacitor terminals.

The voltage in the capacitor splits between the semiconductor and the insulating oxide, considering that, the total capacity (C_t) of the MIS structure shown in Figure 1.3 a), is equal to the capacities of the oxide (C_{ox}) and semiconductor depletion-layer (C_D) associated in series and given by:[36], [38]–[40]

$$\frac{1}{C_t} = \frac{1}{C_{ox}} + \frac{1}{C_D} \tag{1.2}$$

Applying a voltage sweep, the capacitor has three operating domains, I) the accumulation, II) the depletion and III) the inversion regions as shown in Figure 1.3 b).

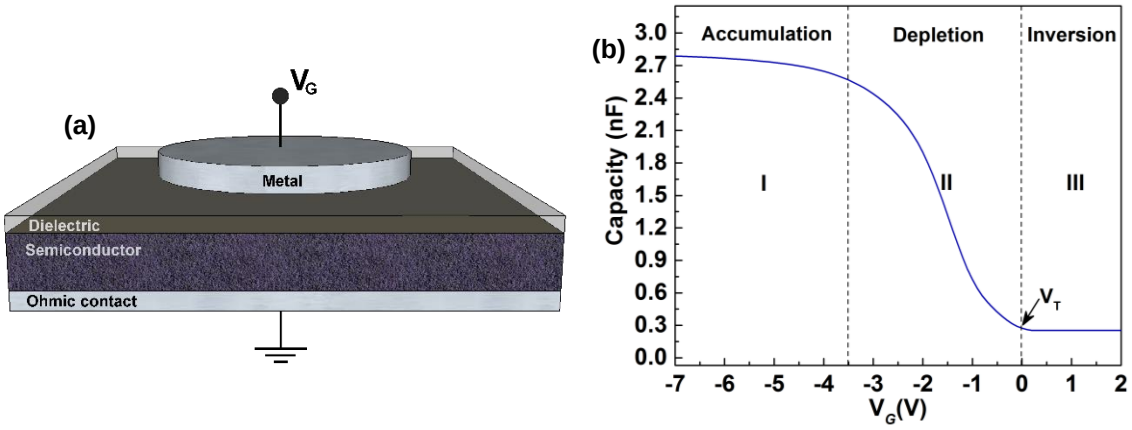

Figure 1.3 – a) MIS structure b) Example of a typical CV curve for a p-type silicon semiconductor based MIS.

I) With no voltage applied, a p-type semiconductor has holes (majority carriers) in the valence band. When a negative voltage (V_G) is applied between the metal gate and the semiconductor, more holes will appear in the valence band at the oxide-semiconductor interface. This is because the negative charge of the metal causes an equal net positive charge to accumulate at the interface between the semiconductor and the oxide (dielectric). This state of the p-type semiconductor is called accumulation. For a p-type MIS capacitor, the total capacity (C_t) in this region is given by the oxide capacity (C_{ox}) because the capacitor behaves as one parallel plate capacitor. [38], [41]

II) Then the majority carriers are repelled from the semiconductor-oxide interface, when a positive voltage (V_G) is applied between the gate and the semiconductor. This state of the semiconductor is called depletion because the surface of the semiconductor is depleted of majority carriers. This area of the semiconductor acts as a dielectric because it can no longer contain or conduct charge. The total measured capacity (C_t) now becomes the oxide capacity (C_{ox}) and the depletion layer capacity (C_D) in series, and as a result, the measured capacity decreases. [38], [41]

III) As the gate voltage (V_G) of a p-type MIS capacitor increases beyond the threshold voltage (V_T), the depletion region reaches a maximum depth and further gate-voltage increases do not further deplete the semiconductor. The positive gate voltage attracts electrons (minority carriers) towards the gate. These minority carriers accumulate at the silicon/oxide interface. The accumulated minority-carrier layer is called the inversion layer because the carrier polarity is inverted. When the depletion region reaches a maximum depth, the capacity is measured by the oxide capacity (C_{ox}) in series with the maximum depletion capacity (C_D). This capacity is often referred to as minimum capacity.[38], [41]

1.4 Thin-Film Transistors

Thin-film transistor (TFT) is a field effect transistor (FET) with three electrodes, the gate electrode which functions as a switch to open or close the other two electrodes, the source and drain, where a vertical electrical field is applied to form a conducting channel. Therefore this device is normally used as an electronic switch, as an example, to turn on or off the pixels of active matrix liquid crystal displays (LCDs) or organic light-emitting diode (OLEDs). The structure is similar a MOSFET built on silicon-on-insulator, the difference is that the active layer is a thin film and the substrate can be of any form, such as a flexible substrate. Apart from the electrodes, the TFT have two other layers, the semiconductor layer, between the source and drain, where the conduction channel is formed, and the dielectric layer used to isolate the semiconductor from the gate electrode (Figure 1.4). [42], [43]

The most common TFTs structures are the staggered and coplanar, each one with two configurations, the top-gate and bottom-gate, depending if the gate electrode is on top or bottom of the structure.[44] Silicon can be used to act as substrate and gate electrode in a staggered bottom-gate configuration, shown in Figure 1.4.

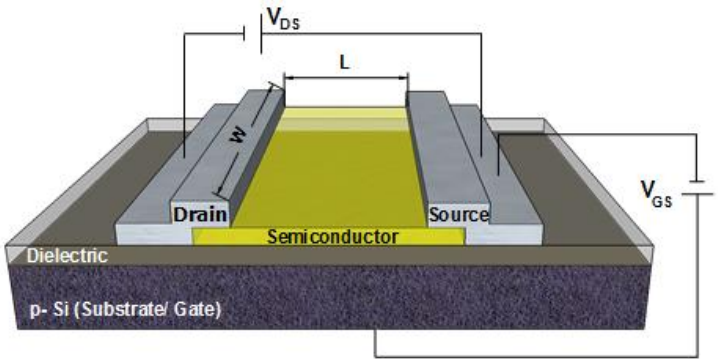

Figure 1.4 – Structure of a TFT in a configuration staggered bottom-gate with the region of the channel depicted, the length (L) and the width (W).

The ideal operation of an n-type TFT depends on the existence of an electron accumulation layer at the dielectric/semiconductor interface. This is achieved for a gate voltage (V_{GS}) higher than a certain threshold voltage (V_T), corresponding to downward band-bending of the semiconductor close to its interface with the dielectric. For $V_{GS} > V_T$, provided that a positive drain voltage (V_{DS}) is applied, current flows between the drain and source electrodes (I_{DS}), corresponding to the *on*-state of the TFT. For $V_{GS} < V_T$, regardless of the value of V_{DS} the upward band-bending of the semiconductor close to the interface with the dielectric is verified, resulting in a low I_{DS} that corresponds to the TFT *off*-state.[44]–[46] Depending on V_{DS}, different operation regimes can be observed during the on-state:

- The linear regime, being I_{DS} described by:

$$I_{DS} = \frac{W}{L} C_i . \mu_{FE} \left[(V_{GS} - V_T) V_{DS} - \frac{1}{2} {V_{DS}}^2 \right], \text{when } V_{DS} < V_{GS} - V_T \tag{1.3}$$

where C_i is the gate capacity per unit area, μ_{FE} is the field-effect mobility, W is the channel width and L is the channel length. For very low V_{DS}, the quadratic term can be neglected, yielding a linear relation between I_{DS} and V_{DS}. In this case, the accumulated charges are considered to be uniformly distributed throughout the channel. [44]–[46]

- The saturation regime, being I_{DS} described by:

$$I_{DS} = \frac{W}{2L} C_i . \mu_{sat} (V_{GS} - V_T)^2 , \text{when } V_{DS} > V_{GS} - V_T \tag{1.4}$$

where μ_{sat} is the saturation mobility. In this regime, the semiconductor close to the drain region becomes depleted, a phenomenon designated by pinch-off that leads to the saturation of I_{DS}.

The static characteristics of TFTs are accessed by their output and transfer characteristics, depicted in Figure 1.5 a) and b), respectively.

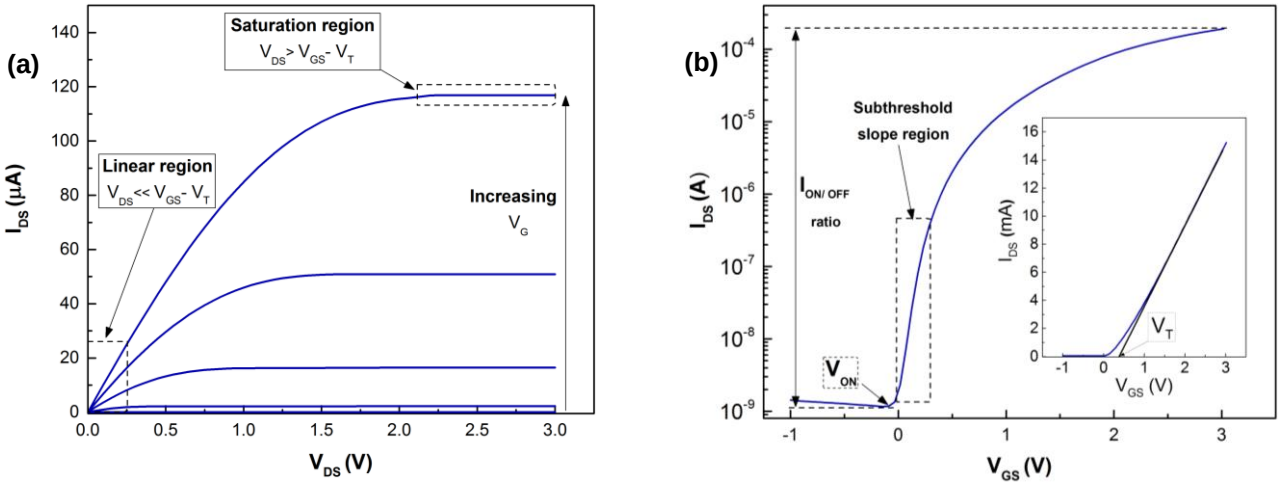

Figure 1.5 – Typical a) output and b) transfer characteristics of a n-type oxide TFT with the threshold voltage (V_T).

In the output characteristics, V_{DS} is swept for different V_{GS} values, allowing one to observe clearly the linear and saturation regimes described above. The transfer characteristics, where V_{GS} is swept for a constant V_{DS}, permit one to extract a large number of quantitative electrical parameters, like On/Off ratio[1], V_T, turn-on voltage[2] (V_{on}), mobility[4] (μ) and subthreshold slope[3] (S) mentioned below. [44]–[46]

$$S = \left(\left|\frac{\partial \log(I_D)}{\partial V_{GS}}\right|\right)^{-1}_{máx} \tag{1.5}$$

Mobility of a TFT can be extracted using different methods, which are described below:

- Field-effect mobility (μ_{FE}) – obtained from the transconductance (g_m) with low V_D:

$$\mu_{FE} = \frac{g_m}{\frac{W}{L} C_i . V_{DS}} \tag{1.6}$$

- Saturation mobility (μ_{sat}) – obtained from the transconductance with high V_D:

$$\mu_{sat} = \frac{\left(\frac{\partial \sqrt{I_{DS}}}{\partial V_{GS}}\right)^2}{\frac{W}{2L} C_i} \tag{1.7}$$

[1]Defined as the ratio of the maximum to the minimum I_{DS}.

[2]The concept of is widely used in the literature, simply corresponding to the V_{GS} at which I_{DS} starts to increase as seen in Figure 1.5 b).

[3]The inverse of the maximum slope of the transfer characteristic, it indicates the necessary V_{GS} to increase I_{DS} by one decade.

[4] Mobility is related to the efficiency of carrier transport in a material, affecting directly the maximum I_{DS} and operating frequency of devices.

2. Materials and Methods

In order to study the aluminum oxide dielectric produced by solution, the synthesis parameters and the annealing temperature of the films were changed with and without far ultraviolet (FUV) exposure. In case of using the FUV the exposure time and distance were altered. For a better understanding of the dielectric in TFTs the standard semiconductor GIZO developed by the research group of CENIMAT was used.[47] Solution-based ZTO and In_2O_3 [35], [48] semiconductors were combined with optimized solution-based AlO_x, in order to achieve fully solution-based TFTs.[35], [48]

2.1 Precursor Solutions Preparation and Characterization

The dielectric precursor solutions were prepared with aluminum nitrate nonahydrate ($Al(NO_3)_3 \cdot 9H_2O$, Fluka, 98%) or aluminum chloride hydrated ($AlCl_3.6H_2O$, BDH Chemicals, 97%) dissolved in 2-methoxyethanol (2-ME, $C_3H_8O_2$, ACROS Organics, 99%), in a concentration of 0.1 M. For combustion reaction precursor solutions, the fuels, urea ($CO(NH_2)_2$, Sigma, 98%) or citric acid ($C_6H_8O_7$, Sigma, >99.5%) were added to the prepared solutions which were maintained under constant stirring for at least 1 h.

For aluminum nitrate based precursors the urea or citric acid to aluminum nitrate molar proportion was 2.5:1 and 0.83:1, respectively, to guarantee the redox stoichiometry of the reaction (Annex A).

Aluminum chloride based precursors were maintained under constant stirring for 12 h. Then oxidizing agents, ammonium nitrate (NH_4NO_3, Roth, 98%) or silver nitrate ($AgNO_3$, Roth, 99%), and the fuels were added. For solution with ammonium nitrate precursor, the urea or citric acid molar proportion was 1:1 and 0.33:1, respectively. In case of solution with silver nitrate the molar proportion of fuels was 2.5:1 and 0.83:1, respectively. Before the addition of fuels these solutions were centrifuged for 4 min at 4000 rpm (Focus instruments, model F140) to remove AgCl formed. (Annex A)

The semiconductor precursor solutions of ZTO were prepared by mixing zinc oxide and tin oxide precursor solutions in a 2:1 proportion. Zinc oxide precursor solution was obtained by dissolving zinc nitrate hexahydrate ($Zn(NO_3)_2 \cdot 6H_2O$, Sigma, 98%) and urea in a 1:1.6 proportion in 2-ME, to yield solutions with 0.05M concentration. Tin oxide precursor solutions were prepared by dissolving tin chloride ($SnCl_2 \cdot 2H_2O$, Sigma, 98%), urea and ammonium nitrate (NH_4NO_3, Roth, 98%) in a 1:1:1 proportion in 2-methoxyethanol, to yield solutions with 0.05 M concentration. Individual solutions were magnetically stirred for 1 h at room temperature in air.[48]

Indium oxide precursor solution was prepared by dissolving indium nitrate ($In(NO_3)_3.xH_2O$, Sigma, 99.9%) in 2-ME for inks with 0.2 M concentration. All precursor solutions were stirred at 430 rpm in air environment at room temperature, to a volume of 10 mL and were filtrated through 0.20 µm hydrophilic filters.[35]

Thermal and chemical characterization of precursor solutions were performed by thermogravimetry and differential scanning calorimetry (TG-DSC) and Fourier Transform Infra-Red (FTIR) spectroscopy. TG-DSC analysis were performed under air atmosphere up to 500 °C with a 5°C/min heating rate in an aluminum crucible with a punctured lid using a simultaneous thermal analyzer, Netzsch (TG-DSC - STA 449 F3 Jupiter). FTIR data were recorded using an Attenuated Total Reflectance (ATR) sampling accessory (Smart iTR) equipped with a single bounce diamond crystal on a Thermo Nicolet 6700 Spectrometer. The spectra were acquired with a 45° incident angle in the range of 1800−540 cm^{-1} and with a 4 cm^{-1} resolution.

2.2 Thin Film Deposition and Characterization

Prior to deposition all substrates (silicon wafer and soda-lime glass with an area of 2.5×2.5 cm^2) were cleaned in an ultrasonic bath at 60 °C in acetone for 10 min, then in 2- isopropanol for 10 min and dried under N_2; followed by a 10 min UV/Ozone surface activation step for a distance lamp of 5 cm using a PSD-UV Novascan system. Thin films were deposited by spin coating a single layer of all the Al_2O_3 precursor solutions (Figure 2.1 a)) with a concentration of 0.1 M for 35 s at 2000 rpm (Laurell Technologies) followed by an immediate hot plate annealing at 350 °C, 250 °C, 200 °C, 180 °C and 150 °C for 30 min in ambient conditions. To study the effect of solution concentration thin films with different concentrations 0.1 M and 0.25 M, were deposited followed by an immediate hot plate annealing for 30 min at 250°C or by combining a short-wavelength far ultraviolet (FUV) photochemical activation with a lamp (H2D2 light source unit, model L11798) at a distance of 9 cm with conventional thermal annealing for 30 min in N_2 condition. To study the influence of annealing at 200 °C, 180 °C and 150 °C thin films with a solution concentration of 0.1 M were deposited followed by combining a FUV exposure at different lamp distances, 9 cm, with a thermal annealing of 30 min, and 5 cm with a thermal annealing at different times, 15 min and 30 min (Figure 2.1 b) and c)). Just for 180 °C was deposited a thin film followed by 2h in PSD-UV Novascan surface activation step to a distance lamp of 2 cm.

The films structure was assessed by glancing angle X-ray diffraction (GAXRD) performed by an X'Pert PRO PANalytical powder diffractometer using with Cu Kα line radiation (λ = 1.540598 Å) with angle of incidence of the X-ray beam fixed at 0.9°. The surface morphology was investigated by atomic force microscopy (AFM, Asylum MFP3D) and scanning electron microscopy (SEM, Zeiss Auriga Crossbeam electron microscope). A cross section of produced devices was performed by focused ion beam (FIB). In FIB milling experiments, Ga^+ ions were accelerated to 30 kV at 5 pA and the etching depth was around 200 nm. Spectroscopic ellipsometry measurements to determine the thickness of thin films deposited on silicon substrates were made over an energy range of 1.5−6.0 eV with an incident angle of 70° using a Jobin Yvon Uvisel system.[49] ATR FT-IR spectroscopy characterization of thin films deposited on Si substrates was performed as described for precursor solutions. The optical properties were obtained using a Perkin Elmer lambda 950 UV/VIS/NIR spectrophotometer. The absorbance (A) was obtained from 190 to 800 nm and the transmittance (T) was obtained from 200 nm to 1450 nm.

2.3 Electronic Device Fabrication and Characterization

Metal−insulator-semiconductor (MIS) capacitors were produced by Al_2O_3 thin film deposition onto p-type silicon substrates (1−10 Ω cm) as described above (see section 2.2). Aluminum gate electrodes (100 nm thick) with an area of 7.85 × 10^{-3} cm^2 were deposited by thermal evaporation via shadow mask. A 100 nm thick aluminum film was also deposited on the back of the silicon wafer to improve electrical contact. Electrical characterization was performed measuring both the capacitance−voltage and capacitance-frequency characteristics in the range of 10 kHz to 1 MHz of the devices using a semiconductor characterization system (Keithley 4200SCS).

The TFTs were produced in a staggered bottom-gate, top-contact structure by depositing Al_2O_3 thin films onto p-type silicon substrates (1−10 Ω cm) as described above. The zinc tin oxide (ZTO) semiconductor layer was deposited by sequentially spin coating (for 35 s at 2000 rpm) four layers of ZTO precursor solution 0.05 M onto the Al_2O_3 thin films and annealed in air at 350 °C for 30 min after each layer deposition.[48] The indium oxide (In_2O_3) semiconductor was deposited by spin coating (for 5 s at 500 rpm followed by 45 s at 6000 rpm) one layer of In_2O_3 precursor solution 0.2 M onto the Al_2O_3 thin films and annealed at 200 °C, 180 °C, 150 °C by combining FUV exposure (distance 5 cm) with thermal annealing at different times, 15 min and 30 min.[35]

The GIZO semiconductor film was sputtered onto the Al_2O_3 thin films via shadow mask (Figure 2.1 d)), from a commercial ceramic target ((LTS Chemical) Inc.) by rf magnetron sputtering

without intentional substrate heating in an AJA 1300-F system. The GIZO deposition parameters were a composition target of 1:2:1, an Air:O_2 flow ratio of 14:2, a pressure deposition 0.3 Pa, a power of 100 W and a deposition time of 13 min 30 sec to obtain a 30 nm thickness.[47]

Finally, source and drain aluminum electrodes (100 nm thick) were deposited by thermal evaporation via shadow mask onto annealed films (Figure 2.1 e)), defining a channel width (W) and length (L). Hereafter the GIZO TFTs with the dielectric layers produced at 150 °C were annealed at 150 °C and all others were annealed at 180 °C, for 1h in air. A 100 nm thick aluminum film was also deposited on the back of the silicon wafer to improve electrical contact and in the flexible substrate of Polyethylene terephthalate (PET) as gate electrode using mechanical masks. The current−voltage characteristics of the devices were obtained in continuous mode with both back and forth sweeps recorded in ambient conditions inside a Faraday cage using a semiconductor parameter analyzer (Agilent 4155C).

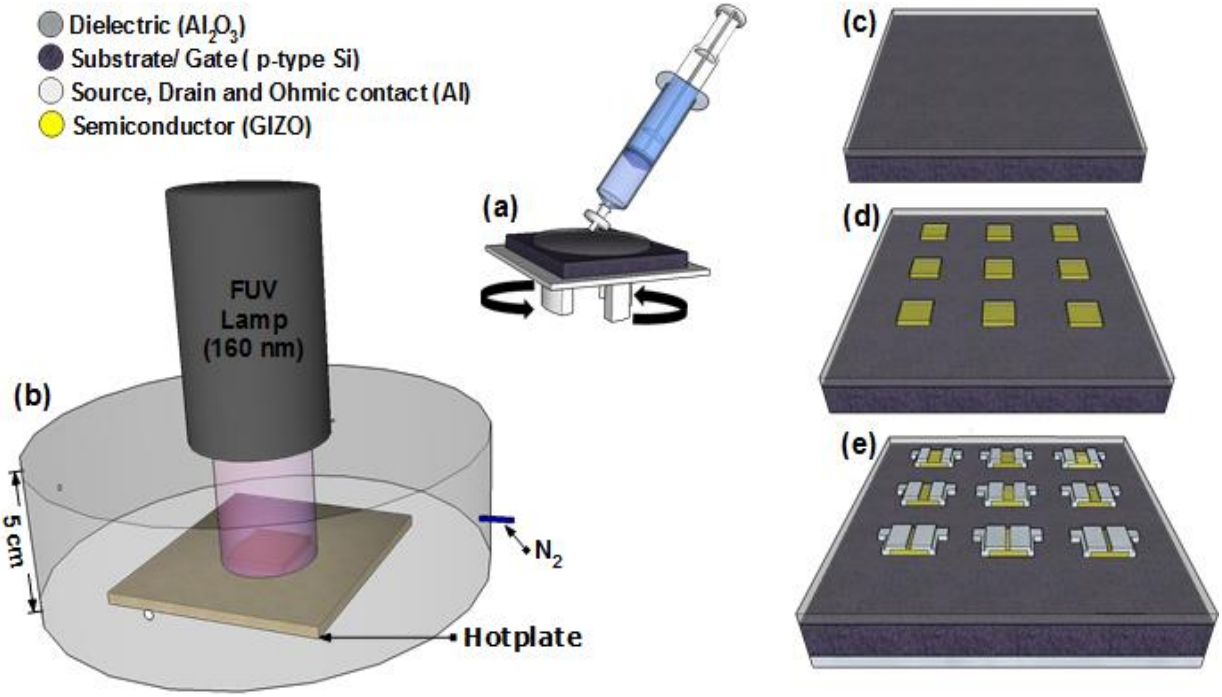

Figure 2.1 – Fabrication of GIZO TFTs with dielectric by solution-based after the cleaning process: a) Deposition of Al_2O_3 precursor solution by spin coating; b) Thermal annealing of dielectric assisted by FUV exposure; c) Dielectric after the anneling treatment; d) After sputtering deposition of GIZO via shadow mask; e) Final TFTs with different channels after source and drain deposition.

Gate bias stress tests were performed on TFTs produced at 180 °C (combining 30 min FUV exposure with thermal annealing) under vacuum environment in a semiconductor characterization system (Keithley 4200SCS). Transfer characteristics were measured at different times during stress and recovery processes, in the dark.

3. Results and Discussion

This chapter discusses the results regarding the solutions characterization, the thin films characterization and the electric characterization of MIS capacitors and TFTs.

3.1 Solutions characterization

3.1.1 Thermal characterization

Thermal analysis of precursor solutions was performed to investigate the decomposition behavior of the metal oxide precursors. Figure 3.1 shows the differential scanning calorimetry (DSC) and thermogravimetry (TG) results for aluminum nitrate ($(Al(NO_3)_3$), with and without combustion in 2-Methoxyethanol (2-ME), and semiconductors In_2O_3 and ZTO precursors up to 350 ºC, since above this temperature no further events were observed.

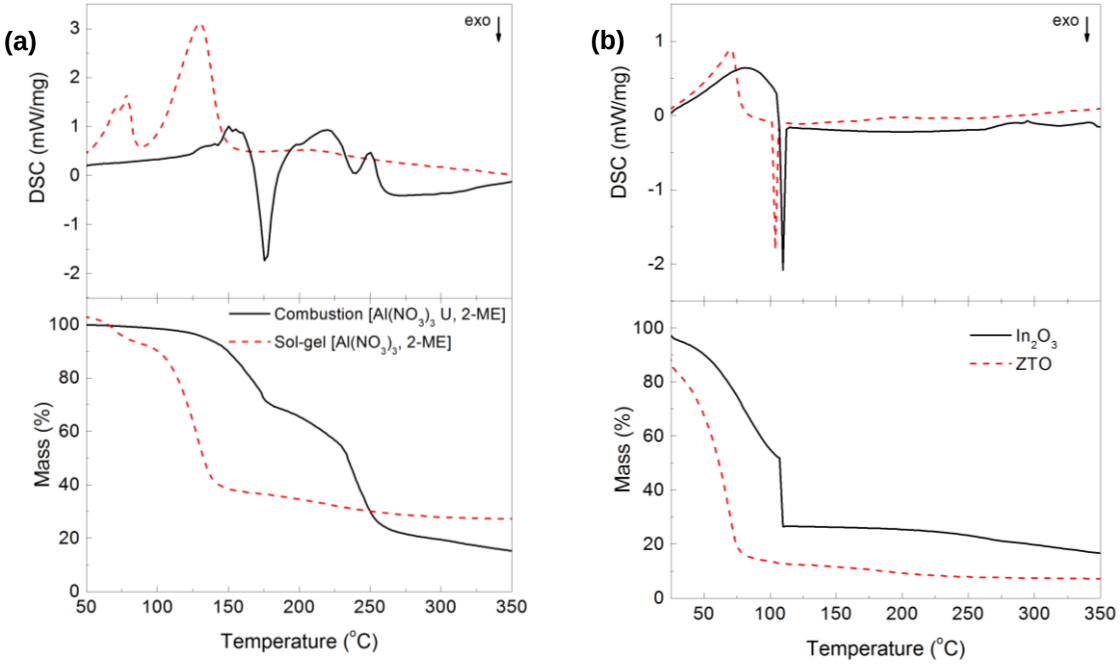

Figure 3.1 – TG-DSC analysis of a) aluminum nitrate precusor ($Al(NO_3)_3$ using urea (U) as fuel or not, and semiconductors b) In_2O_3 and ZTO based precursor solutions using 2-methoxyethanol (2-ME) as solvent.

As depicted in Figure 3.1 a), aluminum nitrate precursor solution with urea shows an intense exothermic peak which is obtained at 176 °C, and a smaller endothermic peak at 250 °C attributed to the degradation of residual organics. Aluminum nitrate precursor solution without any fuel does not show any exothermic peak, only endothermic peaks, at 78 °C, 79 °C and 131 °C with corresponding abrupt mass loss where the solvent evaporation occurs. In that case the reaction is not exothermic because there is no fuel.

For different semiconductors In_2O_3 and ZTO precursor with the same solvent 2-ME, Figure 3.1 b), exhibit an intense exothermic peak with corresponding abrupt mass loss, at 110 °C and 104 °C, respectively, which is attributed to the combustion reaction of the organic fuel with the metal nitrates. In case of In_2O_3 it is not necessary have fuel to form the exothermic peak.

Thermal analysis of the precursor solutions indicate that the minimum temperature required for full degradation is 250 °C in case of aluminum nitrate precursor solution with urea. For that ultraviolet (UV) irradiation was used on annealing process to reduce the temperature required because that aid on the degradation of residual organics.

3.1.2 Optical characterization

In order to know if aluminum precursor solutions absorb UV irradiation due to the use of UV lamps in combination with the annealing of the films the absorbance of all the solutions in that region was measured from 190 nm to 400 nm. Figure 3.2 shows that all the solutions show absorption peaks between 400-200 nm.

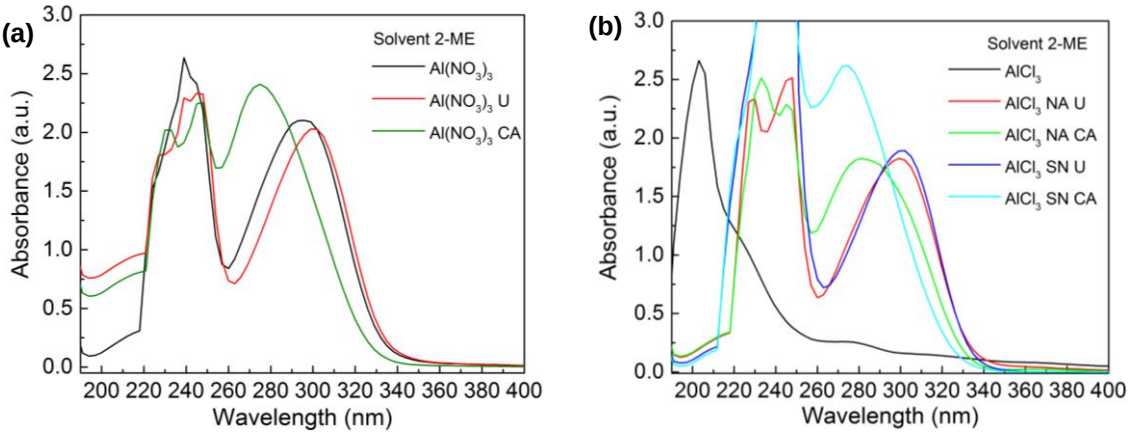

Figure 3.2 – Absorbance spectra of all aluminum oxide precursor solutions: a) Aluminum nitrate using urea (U) or citric acid (CA) as fuel and without; b) Aluminum chloride with nitrate precursors, ammonium nitrate (NA) or silver nitrate(SN) and without. In the aluminum chloride solutions with nitrate precursors U or CA was used as fuel.

The absorption peaks for the different solutions are depicted in Table 3.1. The solutions shown in Figure 3.2 with nitrate precursors without being silver nitrate (SN) precursors (saturated in that region) or aluminum chloride precursor ($AlCl_3$), absorb near the peak which has higher intensity of DUV lamp, 253.7 nm. Taking that into account one film with the solution of aluminum nitrate ($Al(NO_3)_3$) with urea using this lamp was produced. In relation to the UV lamp more used in this work cannot know much information about the absorption of the same solutions because the main peak of this stands at 160 nm (Annex B), which is not possible to measure the absorbance of this equipment that is limited by 190 nm and by the cuvette cell material.

Table 3.1 – Main absorption peaks of all aluminum precursor solutions.

Solution	Main Peaks (nm)		Solution	Main Peaks (nm)
$Al(NO_3)_3$	(239); (296)		$AlCl_3$ NA U	(248); (299)
$Al(NO_3)_3$ U	(245); (299)		$AlCl_3$ NA CA	(233); (281)
$Al(NO_3)_3$ CA	(248); (275)		$AlCl_3$ SN U	(302)
$AlCl_3$	(203)		$AlCl_3$ SN CA	(275)

3.2 Thin films characterization

3.2.1 Optical characterization

3.2.1.1 Thickness of dielectric thin films

The thickness of all dielectric thin films was measured by ellipsometry due to their small thickness. For alumina thin films annealed at 350 ºC with different precursor solutions for a concentration of 0.1 M, with and without fuel, the thickness of the dielectric thin films had an average of 12 ± 1 nm. The thickness of aluminum chloride film without nitrate precursors is not accounted on average due to the presence of chlorides in the film which contributes to a higher thickness and less uniformity, as can be seen in the attached image depicted in Annex C. For a higher concentration of 0.25 M the thickness of the film increased as expected, being around of

30 nm. In all the other conditions for a concentration of 0.1 M with FUV irradiation, the thickness of the films was around 12 nm and without were slightly higher, as shown on table of Annex C.

3.2.1.2 Transmittance

The transmittance of alumina thin films with different processing conditions and In_2O_3 were measured on glass between 190 nm and 1450 nm with a wavelength step of 3 nm. By analysing the Figure 3.3 a) it was observed that transmittance is around 91% for alumina thin films regardless of using fuel or not at 350 ºC and 90% for In_2O_3 thin films at 200 ºC , Figure 3.3 b), between 400 nm and 1450 nm. For low temperatures the thin films with different processing conditions showed the same transparency in visible region (Annex D).

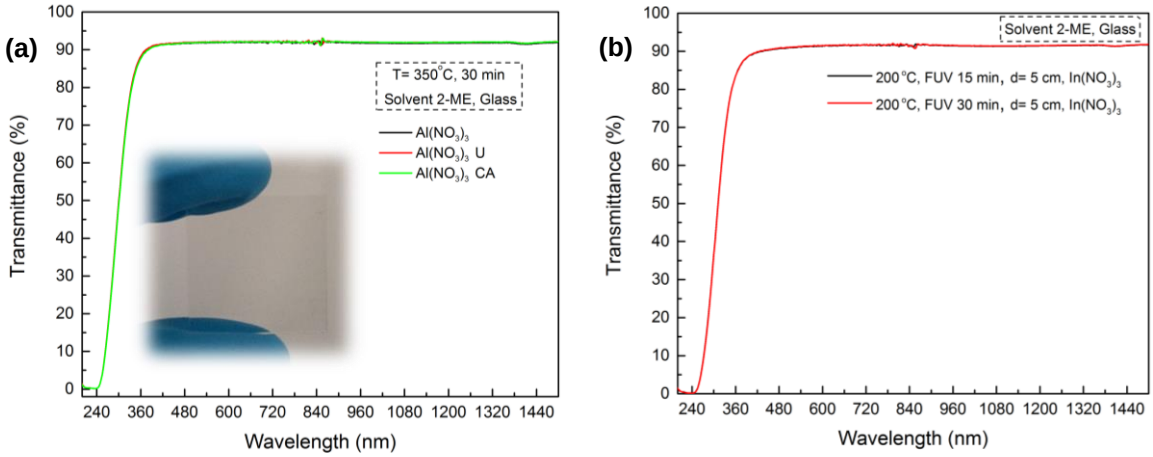

Figure 3.3 – Transmittance spectra of thin films in a glass substrate: a) Alumina dielectric using the same precursor solution without and with fuel (U or CA) at 350 ºC and b) In_2O_3 semiconductor precursor solution at 200 ºC with assistance of far ultraviolet (FUV) treatment for different exposure times, 15 and 30 min.

3.2.1.3 Fourier transform infrared spectroscopy (FTIR)

The FTIR spectra of alumina dielectric thin film was performed to identify the elements through characteristic spectra. The spectra of dielectric thin films for several processing temperatures and for solutions with different processing conditions deposited on silicon substrates were measured using the attenuated total reflectance (ATR). Data are presented (Figure 3.4) between 2500 and 540 cm^{-1} because above these values no spectral changes are observed.

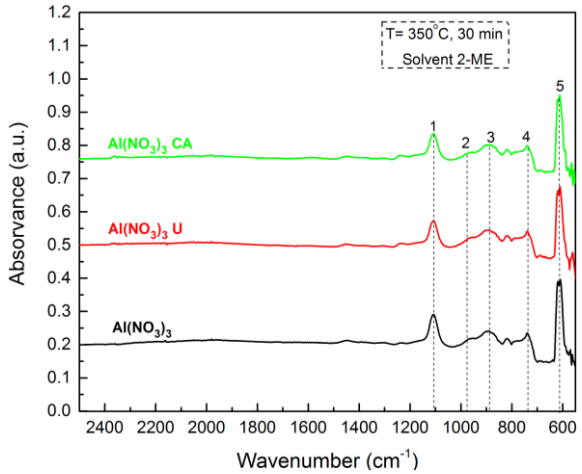

Figure 3.4 – FTIR spectra of alumina dieletric thin films using the same precursor solution with combustion (U or CA) and without at 350 ºC.

Figure 3.4 show the FTIR spectrum of alumina thin films, with variation on the properties of the solutions at 350 ºC. After correction of the atmosphere contribution, the spectra for all samples are found to be similar, with slight changes at low temperatures, showing the CO_2 (between 2390 and 2300 cm^{-1}) and H_2O (between 1700 and 1500 cm^{-1}) bands (Annex E). The absorbance peaks of the thin films that appear between 1000 and 600 cm^{-1} in Figure 3.4 are characteristic of vibrational modes of alumina, as shown in Table 3.2.[50] The present peaks in this spectrum confirm the presence of alumina, essential as dielectric layer. For low temperatures the thin films with different processing conditions were not exhibited because showed similar results although with less intensity (Annex E).

Table 3.2 – Characteristic absorbance peaks and associated vibrational modes of the corresponding chemical bonds for the spectrum of alumina thin film on silicon.[50]

Number	Position (cm^{-1})	Mode type	Chemical Bond
1	1107	Transversal Optic Stretching	Si-O
2	968	Longitunal Optic Stretcing	Al-O
3	889	Condensed Tetraedra	$Al-O_4$
4	739	Condensed Tetraedra Stretching	$Al-O_4$
5	611	Transversal Optic Bending	$Al-O_2$

3.2.2 Structural and morphological characterization

3.2.2.1 X-Ray Diffraction (XRD)

There is a great need to know if the dielectric thin film has an amorphous structure that allow the use of lower temperatures when compared with the polycrystalline structures. Unlike these the amorphous structures do not suffer from grain boundaries allowing to have low leakage currents and present smoother and uniforms films, affording better interface properties.[11]

The absence of diffraction peaks in XRD diffractograms at 350 ºC, shown in Figure 3.5, confirms the amorphous nature of the deposited films on glass, independently of the precursor solutions.

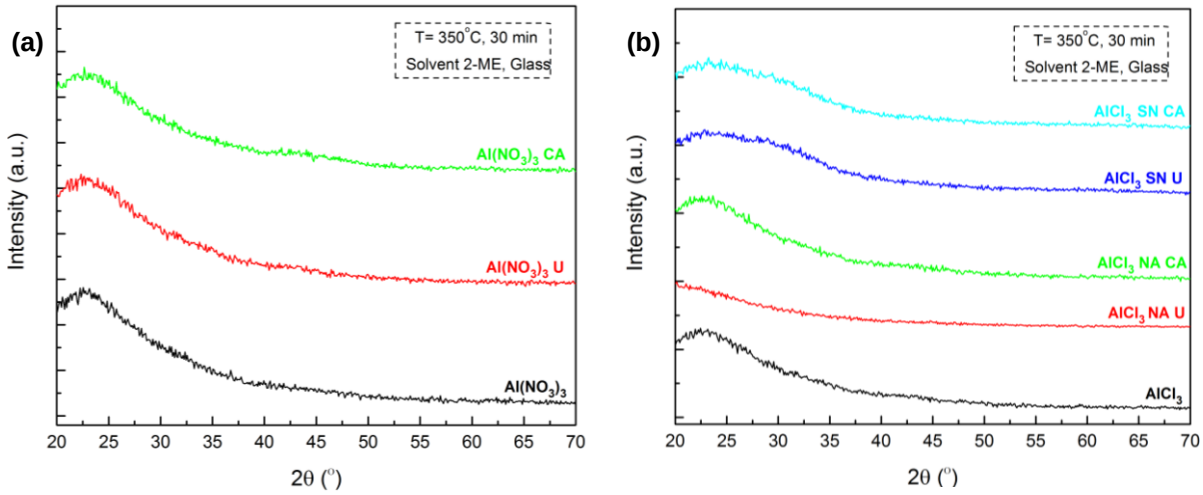

Figure 3.5 – XRD diffractograms of dielectric thin film using different precusors solutions deposited in glass: a) aluminum nitrate without and with combustion (U or CA) and b) aluminum chloride without and with nitrate precursor solutions, silver nitrate (SN) or ammonium nitrate (NA), using U or CA as fuel.

The only peak observed is characteristic of the glass used as a substrate. The films at low processing temperatures show the same characteristics (Annex F), despite being deposited on silicon substrates.

3.2.2.2 Atomic Force Microscopy (AFM) and Scanning Electron Microscope (SEM)

Surface morphology of alumina dielectric thin films, AlO_x, based on aluminum nitrates using urea as fuel in 2-ME and the semiconductor, In_2O_3, deposited onto alumina thin films at different temperatures and annealing conditions, were measured by AFM. The determination of the surface roughness (Rms) was acquired in alternate mode and the topographic images were analysed in data analysis software Gwyddion. Figure 3.6 shows that the roughness of the dielectric thin films increases for low annealing temperatures, however remains below 2 nm which reveals an adequate smooth surface.

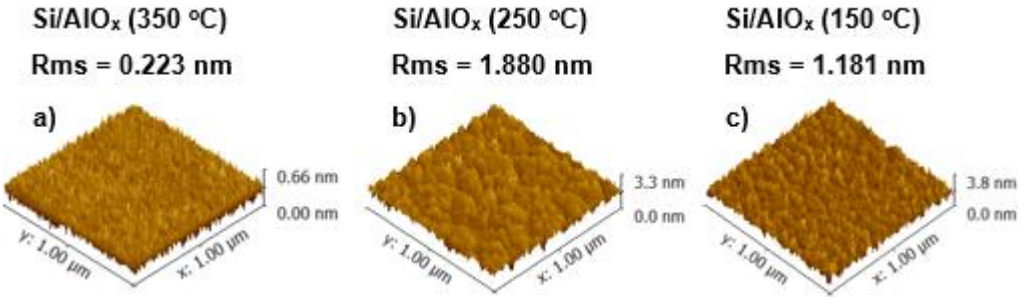

Figure 3.6 – Morphological characterization of 2-methoxyethanol (2-ME) solution based AlO_x thin films for a concentration of 0.1 M. AFM deflection images of 1 × 1 µm^2 to an anneling of 30 min for different temperatures of annealing: a) 350 °C, b) 250 °C and c) 150 °C.

All of the other AlO_x thin films had a surface roughness lower than 2.16 nm for different concentrations and conditions of annealing, shown in Annex G. As the dielectric thin films were used in TFTs with GIZO, ZTO or In_2O_3 as active layer, the surface roughness of TFTs with In_2O_3 semiconductor processed by solution and deposited at low temperatures was studied. Figure 3.7 shows AFM and SEM images of the surface roughness before, Figure 3.7 a), and after, Figure 3.7 b), the deposition of the In_2O_3 semiconductor onto dielectric layer at a temperature of 180 °C (other conditions in Annex G).

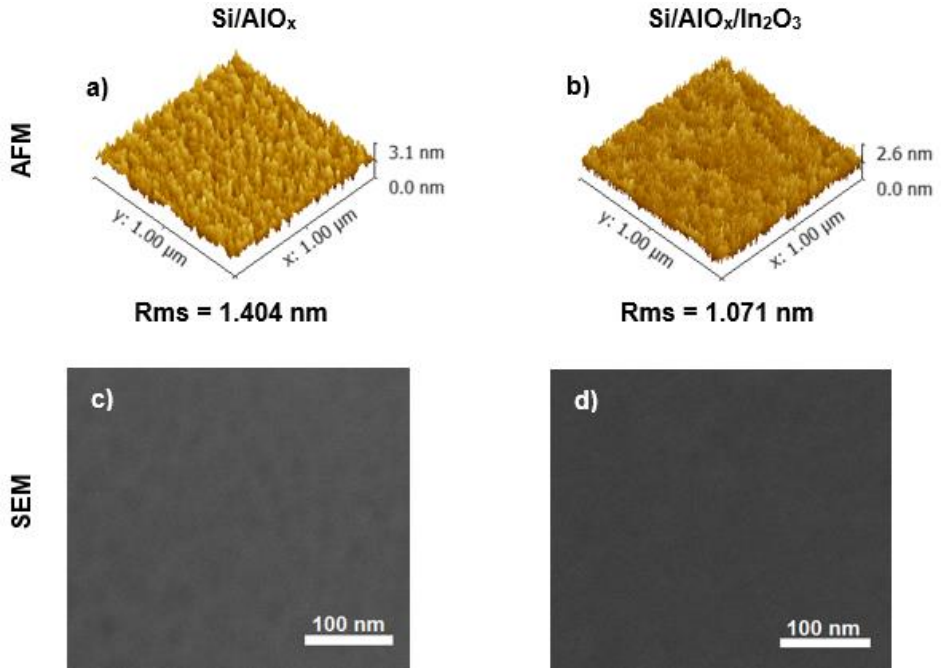

Figure 3.7 – Morphological characterization of thin films produced by solution combining FUV treatment to a lamp distance of 5 cm with annealing at 180 °C for 30 min. AFM deflection images of 1 × 1 µm^2 surface area and SEM surface: a,c) AlO_x thin film; b,d) In_2O_3 deposited onto AlO_x thin film.

The films roughness was determined from the AFM height profile of a 1 × 1 μm^2 area scan. AlO_x based films demonstrate a higher surface roughness, 1.404 nm, than In_2O_3 deposited onto AlO_x thin films, 1.071 nm. But such differences are not significant due to AlO_x films were only measured after two months of production which can influence the roughness due to exposure of the samples in air. Nevertheless smooth and uniform films are obtained for the AlO_x, Figure 3.7 c), and AlO_x/ In_2O_3 thin films, Figure 3.7 d), produced by solution as confirmed by surface SEM images.

The morphology of GIZO TFTs with a solution based dielectric thin film annealed at 180 ^oC for 30 min combined with FUV radiation to a lamp distance of 5 cm were investigated using SEM-FIB. For study the alumina dielectric was chosen GIZO for being a standard semiconductor deposited by sputtering, allowing to focus on the dielectric behavior on TFTs under different conditions. SEM-FIB cross-section images of bottom gate AlO_x/GIZO TFTs produced on highly doped p-Si (gate) with aluminum source/drain contacts clearly show all layers (Figure 3.8).

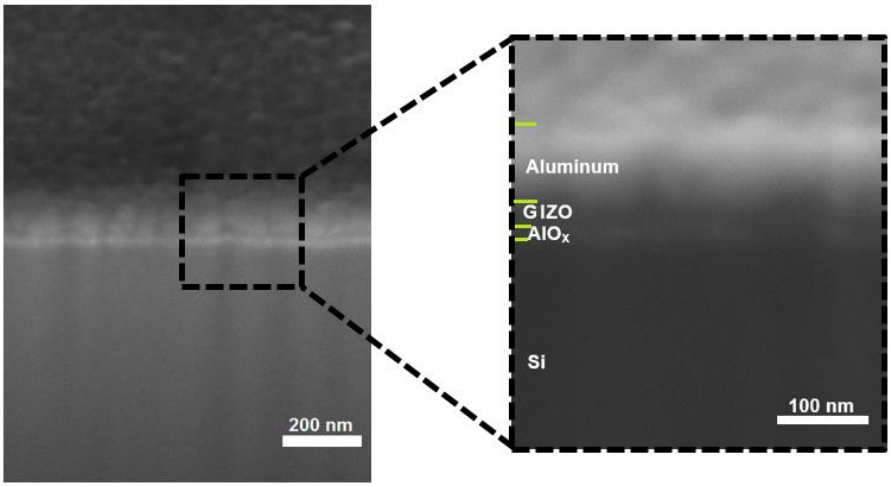

Figure 3.8 – SEM-FIB cross section images of bottom gate AlO_x/GIZO TFTs produced on highly doped p-Si (gate) with aluminum source/drain contacts.

The average thickness of the constituent layers of the TFTs were measured using the program ImajeJ. The thickness of aluminum source/drain contacts and GIZO thin films has on average of 85.2 nm and 27.1 nm, respectively. Comparing the thickness of AlO_x thin film measured by the image of SEM-FIB with the ellipsometry technique was confirmed that the values were similar, 12.2 nm and 11.9 nm, respectively.

All aluminum oxide precursor solutions absorbed in the UV region and the thin films of alumina showed an amorphous nature, transparency (91%) and good uniformity.

3.3 Electrical characterization of solution-based AlO_x capacitors

The quality of TFTs is highly dependent on characteristics of the insulating material and the properties of insulator-semiconductor interface. For this, the insulating layer has been studied using metal-insulator-semiconductor (MIS) structures. The electrical characterization of these structures is done by capacity-voltage (CV), capacity-frequency (Cf) and current-voltage (IV) curves which enable to acquire information about the dielectric constant and the breakdown field of the dielectric layer.

In the CV curves, the oxide capacity corresponds to the maximum capacity measured in the accumulation region, according to Figure 1.3 b). These curves show hysteresis in a clockwise direction in this work for all the processing temperatures, which is assigned to the trapping of charges in the dielectric layer from the metal. [51] The Cf curves allow to see the changes of capacity with the frequency (in a range of 10 kHz to 1 MHz) to different applied voltages V_{GS} and

the IV curves enable to determine the current behaviour when it passes through the device according to the voltage applied to the gate.

The frequency chosen to measure capacity of the dielectrics was 100 kHz to have all the dielectrics in the same condition because in certain cases for lower frequencies the capacity increases exponentially with the decreasing of frequency, which can be explained by the response time to changes in the applied electric field or due to ionic polarization contribution. This might result in overestimation of the mobility value which is not correct.

3.3.1 Influence of precursor reagents

Firstly the effect of the dielectric thin film for different precursor solutions was tested without and with combustion reaction using urea (U) or citric acid (CA) as organic fuels in 2-methoxyethanol (2-ME) annealed at 350 ºC for 30 min and a concentration of 0.1 M. In Figure 3.9 is displayed the electrical characteristics of MIS capacitors produced with aluminum nitrate precursor solution in those conditions.

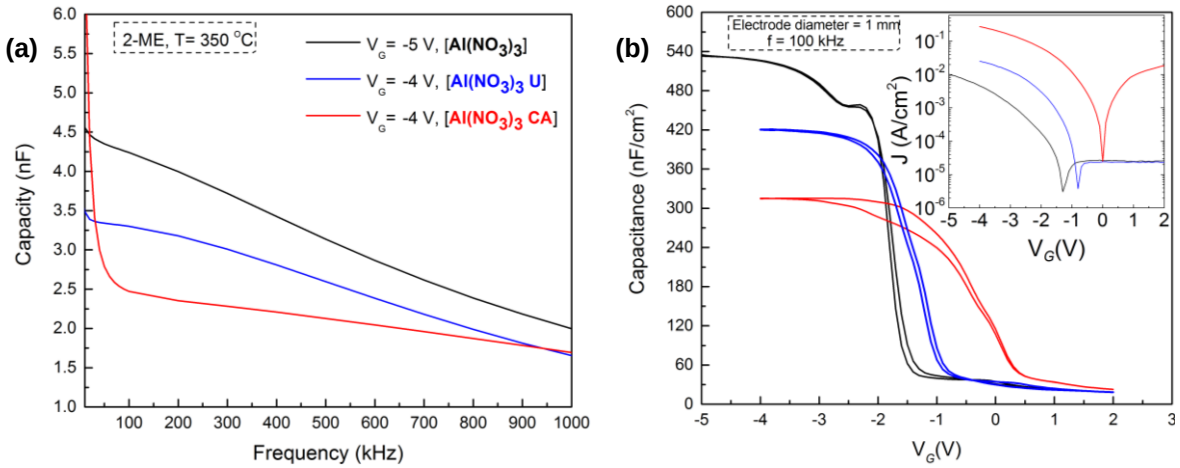

Figure 3.9 – a) Capacity-frequency and b) Capacitance−voltage characteristics with IV curves of p-Si/AlO_x/Al MIS capacitors produced with aluminum nitrate precursor solution without and with combustion using urea (U) or citric acid (CA) as fuels in 2-methoxyethanol (2-ME) annealed at 350 ºC for 30 min to a frequency of 100 kHz.

The capacity of the dielectric using aluminum nitrate precursor solution without fuel is higher and have a bigger variation with frequency when compared with the precursor solutions where the combustion reaction occurs, as shown in Figure 3.9 a). Among the three dielectrics, the one who has the aluminum nitrate precursor solution with citric acid is the worst because have a higher leakage current density (J) and hysteresis, presented in Figure 3.9 b). That can be explained by the size of the citric acid organic molecule when compared to urea, causing low agglomeration of particles when occurs the combustion reaction resulting in a porous film, i.e., less uniform surface.[52]–[54]

The dielectrics with aluminum chloride as precursor solution show a higher hysteresis or a bigger variability of the capacity with frequency, as shown in Annex H. Taking into account all this information the dielectric with aluminum nitrate precursor solution using urea as fuel was chosen, not only because of the electrical characteristics, low hysteresis and lower capacity variation at low frequencies, but also due to the use of nitrates and urea in solution, which helps in the condensation of the films at relatively low temperatures when compared with chloride precursors.[55]

3.3.2 Influence of solution concentration and FUV irradiation

The influence of solution concentration and FUV irradiation was assessed on MIS structures annealed at 250ºC. For different concentrations, 0.1 M and 0.25 M, just thermal annealing of the film or thermal annealing combined with a far ultraviolet (FUV) photochemical activation (lamp distance of 9 cm) were performed. Results are depicted in Figure 3.10. For higher concentrations the capacity is lower due to the increase of the film thickness, Figure 3.10 b), verified by the equation 1.1.

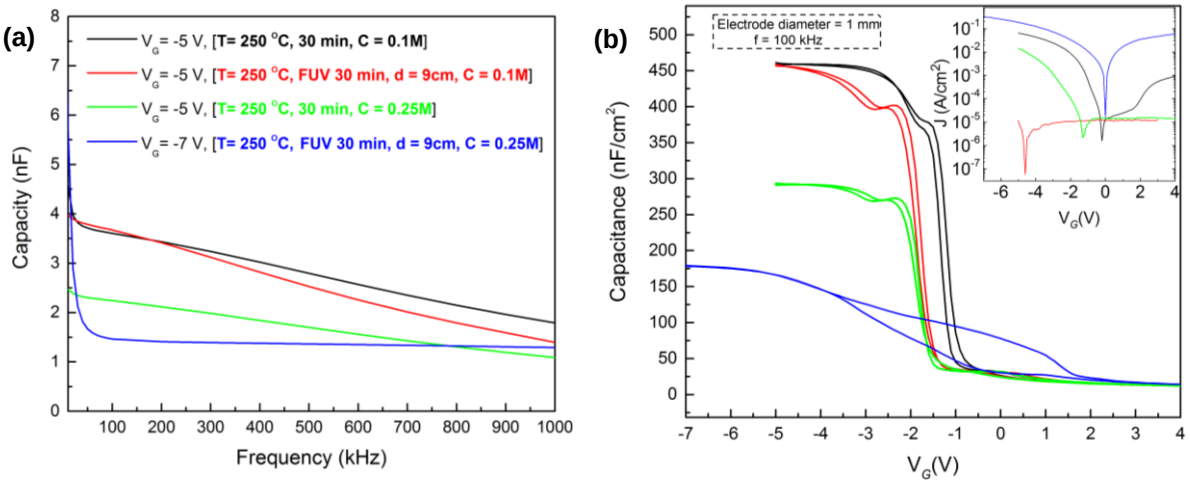

Figure 3.10 – a) Capacity-frequency and b) Capacitance−voltage characteristics with IV curves of p-Si/AlOx/Al MIS capacitors annealed at 250 ºC without and with FUV irradiation for different concentrations to a frequency of 100 kHz.

By using the FUV irradiation combined with thermal annealing for both concentrations expedites film formation, densification, condensation, and impurity decomposition.[34],[35] Therefore the film thickness gradually decreased with the ultraviolet exposure as shown previously in ellipsometry measurements (Annex C). For a higher concentration the capacitor showed a lower capacity variation with frequency, Figure 3.10 a), and the exposure of FUV irradiation is not very efficient resulting in higher hysteresis, Figure 3.10 b). The use of FUV irradiation simultaneously with the thermal annealing worked better at a lower concentration resulting in a lower leakage current density, as depicted in Figure 3.10 b).

3.3.3 Effect of FUV exposure parameters for low temperature annealing

In order to have compatibility with flexible substrates low annealing temperatures, 200 ºC, 180 ºC and 150 ºC, were tried for different annealing conditions. At these temperatures was confirmed that using FUV irradiation helps in reducing hysteresis and on densification of the film. To increase the irradiation intensity a shorter distance of 5 cm to the FUV lamp was tried; causing a lower hysteresis and a smaller variation of capacity with the frequency. Establishing the proper irradiation distance the annealing time was reduced to 15 min to determine if the process would become more compatible with R2R process. To illustrate these conditions the most suitable temperature of 180 ºC was chosen where the dielectric presented a higher performance for a FUV lamp distance of 5 cm (Figure 3.11 a)). The devices produced at 200 ºC and 150 ºC are depicted in Annex H and CV curves showed the same behavior with the implementation of FUV irradiation during annealing.

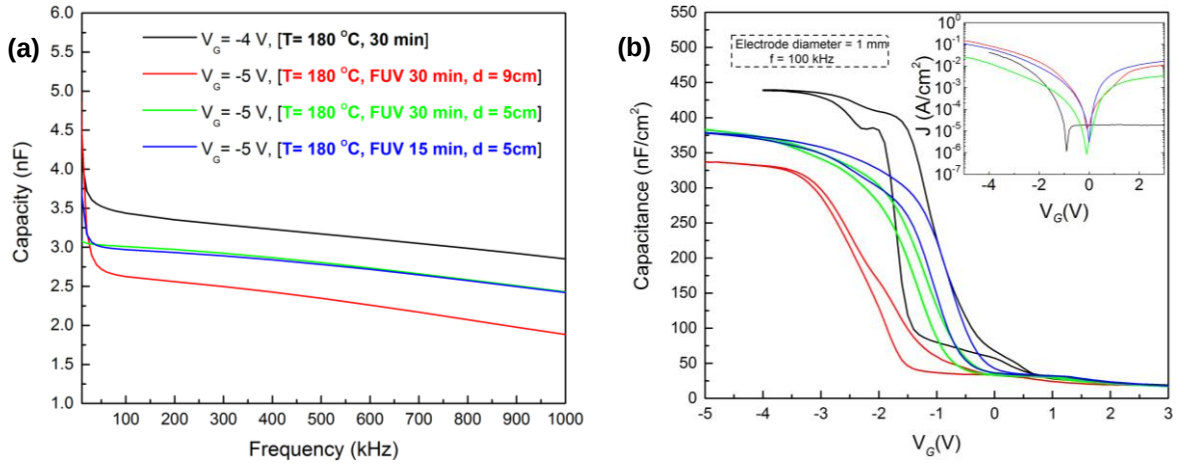

Figure 3.11 – a) Capacity-frequency and b) Capacitance−voltage characteristics with IV curves of p-Si/AlO_x/Al MIS capacitors annealed for different times at 180 ºC with and without FUV irradiation (frequency of 100 kHz).

For shorter annealing (15 min) for 180 ºC curing temperature combined with FUV irradiation; the devices exhibit a large hysteresis in the CV curves and higher capacity at low frequencies Figure 3.11 b) and a), respectively, when compared with the device annealed for 30 min.

It was observed that the hysteresis decreases with the increasing of temperature but can decrease to lower temperatures when FUV irradiation is used.

Most of the films to different temperatures presented a high density of leakage current owing to the presence of fixed charges attributed to structural defects in the dielectric-silicon interface (Figure 3.11 b) and Annex H). The effect of trapped charge in the dielectric, typically located at the interfaces of the constituent layers of the capacitor, must also be considered. But one of the main reasons for leakage current is the low thickness of the dielectric films because when aluminum electrodes are deposited by resistive thermal evaporation can cause short circuits, thus becoming a current path through the dielectric, which contributes to high leakage current. Nevertheless the FUV irradiation helps film densification and a slight decrease of leakage current.

The dielectric constant (Annex C) of the materials were obtained using the equation 1.1, these are lower than expected for Al_2O_3,~9, however, these are in agreement with reported values for solution processed aluminum oxide.[56]

3.4 Electrical characterization of TFTs using AlO_x as dielectric

3.4.1 Influence of the semiconductor layer

The thin film of AlO_x using different precursor solutions in 2-ME has been implemented in TFTs with different semiconductors, ZTO by solution process and GIZO by sputtering, to a temperature of 350 ºC. The TFTs using aluminum chloride as precursor solution showed worse behavior (Annex J) as mentioned earlier in section 3.3.1, when compared TFTs using aluminum nitrate as precursor solution. These are extremely affected by fringing electric field effect because the leakage current is higher or very close to the I_{DS} current and have smaller On/Off ratios.[57] Therefore solutions with aluminum nitrate as precursor solution was chosen for further studies. Figure 3.12 shows the transfer curves of ZTO TFTs, Figure 3.12 a), and GIZO TFTs, Figure 3.12 b), with dielectric based solution for different process conditions and the output curves of each TFTs with aluminum nitrate precursor solution with urea in 2-ME as dielectric, Figure 3.12 c) and d), respectively.

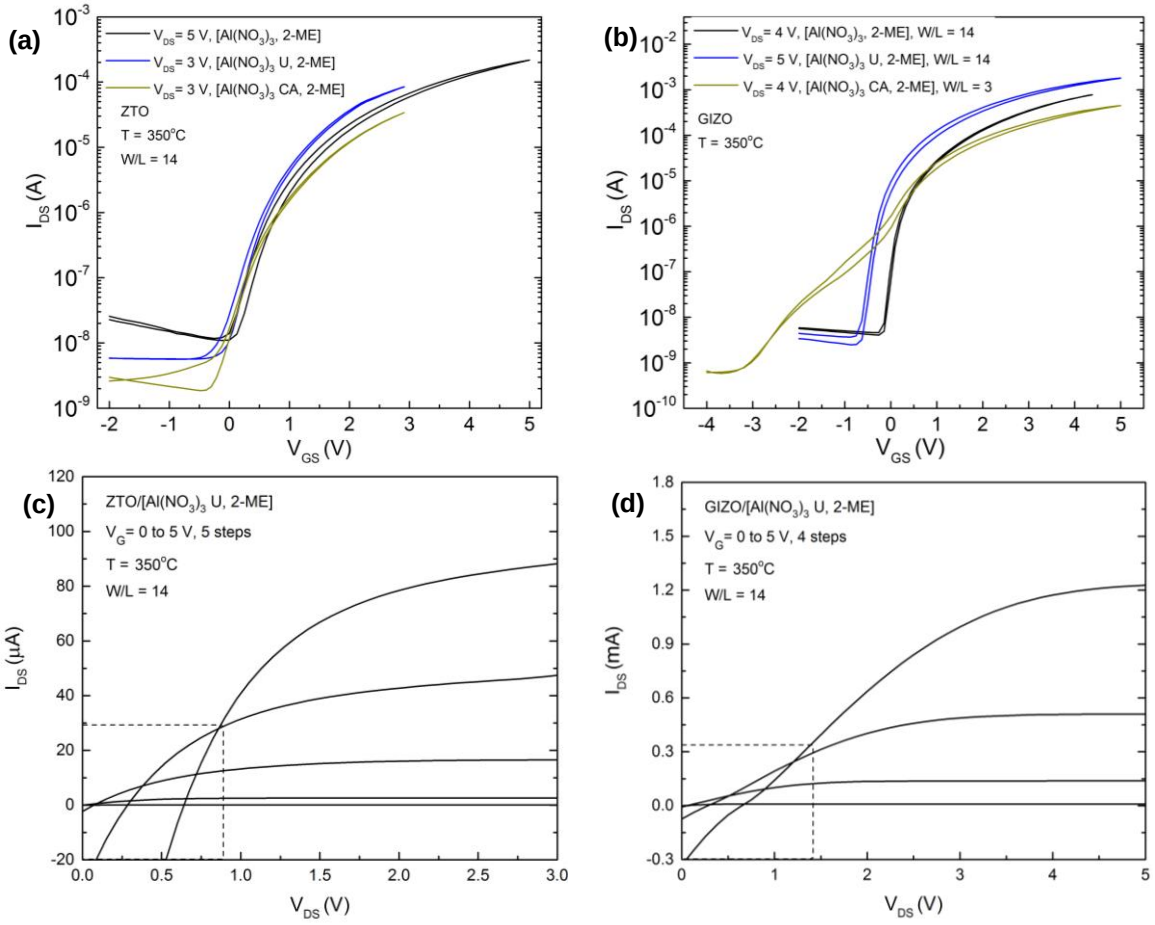

Figure 3.12 – Transfer curves of a) GIZO TFTs and b) ZTO TFTs, with dielectric of aluminum nitrate precursor solution with and without fuel (U or CA) in 2-ME. Output curves using aluminum nitrate precursor solution with urea as dielectric in c) GIZO TFTs and d) ZTO TFTs.

The characteristic parameters presented in Table 3.3 to analyze the performance of the devices were obtained taking into account the equations and graphs mentioned previously in section 1.4. The exact channel widths depicted in Annex I, were measured with an optical microscope.

Table 3.3 – Characteristic parameters of GIZO and ZTO TFTs using ($Al(NO_3)_3$) with (U or CA) and without fuel in 2-ME at 350 ºC.

Semiconductor	Dielectric Solution ($Al(NO_3)_3$)	T=350 ºC							
		$\frac{W}{L}$	Von (V)	I_{ON}/I_{OFF}	V_T (V)	S (V/dec)	μ_{SAT} (cm^2/Vs)	V_{Hyst} (V)	$I_{G\ max}$ (A)
ZTO solution	2-ME	14	-0.25	1.84×10^4	0.63	0.31	3.33	0.13	1.02×10^{-4}
	U, 2-ME	14	-0.84	1.50×10^4	0.48	0.32	6.68	0.17	2.28×10^{-4}
	CA, 2-ME	14	-0.48	1.83×10^4	0.63	0.32	3.61	0.07	5.52×10^{-5}
GIZO sputtering	2-ME	14	-0.26	1.92×10^5	0.44	0.13	14.40	0.03	7.28×10^{-4}
	U, 2-ME	14	-0.88	7.24×10^5	-0.14	0.14	27.93	0.13	9.15×10^{-4}
	CA, 2-ME	3	-3.68	7.67×10^5	0.05	0.55	47.04	0.16	5.22×10^{-4}

Initially ZTO TFTs were produced with all the dielectric solutions of alumina to obtain all solution processed TFTs. The best TFTs obtained were of aluminum chloride precursor ($AlCl_3$) with ammonium nitrate (NA) using urea (U) as fuel (Annex J) and with aluminum nitrate precursor ($Al(NO_3)_3$) solutions without citric acid. Then GIZO TFTs were produced to study more deeply the dielectric. When compared the two different semiconductors, in Table 3.3, was observed that GIZO TFTs were less affected by the fringing electric field resultant of the leakage current, have

a higher On/Off ratio and lower hysteresis for dielectrics with aluminum nitrate precursors, as depicted in Figure 3.12 b).

The higher mobility for both semiconductors was achieved using aluminum nitrate precursor with urea as fuel, since the high mobility of GIZO using $Al(NO_3)_3$ with citric acid (CA) as dielectric solution is the effect of the fringing electric field of using small channel ratio that leads to significantly overestimated field-effect mobility, as shown in Table 3.3 .[57] All the TFTs with dielectric solutions using citric acid as fuel were more affected by the fringing electric field because is formed a porous film in combustion reaction which leads to a high leakage current.[53] The GIZO TFTs have better subthreshold slope than ZTO TFTs due to a greater semiconductor quality and to a lower defects between semiconductor and dielectric, depicted in Table 3.3 and Figure 3.12 a),b).

The devices show significant leakage as depicted by the dashed squares on the output curves of TFTs for both semiconductors, Figure 3.12 c) and d). This is due to unpatterned semiconductor layer and lower I_G can be obtained by patterning the semiconductor, in this case using mechanical masks.[58]

The ZTO semiconductor was not used to proceed for lower temperature because is not optimized for such. Considering the results achieved GIZO and aluminum nitrate precursor with urea were chosen to pursue lower temperatures.

3.4.2 Influence of solution concentration and FUV irradiation

All the devices were patterned when decreasing the annealing temperature of TFTs to 250 ºC resulting in a lower leakage current. For this temperature different concentrations of dielectric solution, 0.1 M to 0.25 M, and different processes of annealing, just thermal annealing or combined with FUV photochemical activation to a lamp distance of 9 cm, were used.

Figure 3.13 a) shows that TFTs for a higher concentration precursors in dielectric, the On current decrease almost one order of magnitude due to the channel size whereas the hysteresis, the subthreshold slope, the threshold voltage and saturation mobility are higher. The highest mobility is explained due to the film has a greater thickness that makes the capacity being smaller, as shown in equation 1.1. The V_{on} stay more close to zero for a highest concentration, as shown in Table 3.4.

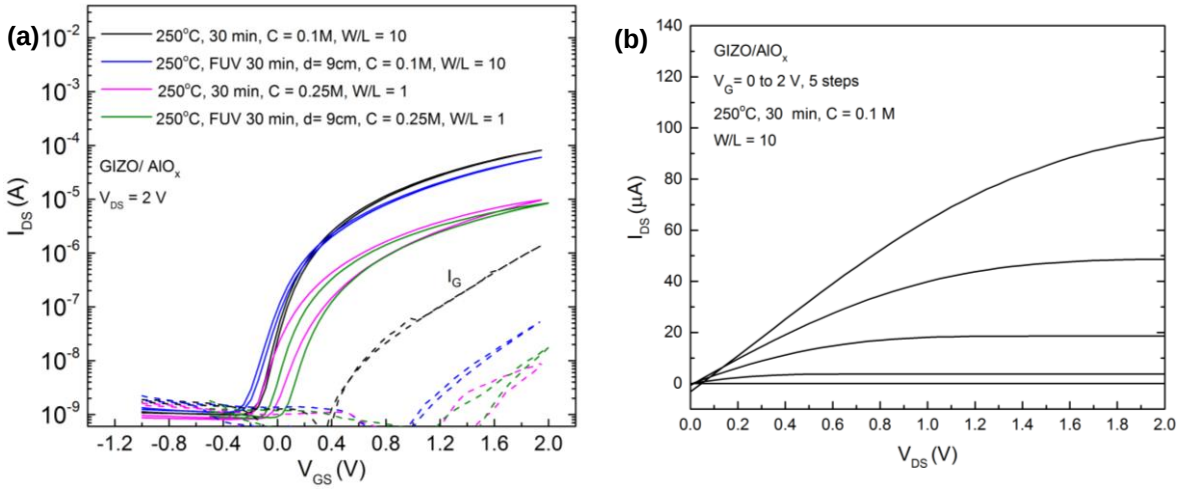

Figure 3.13 – a) Transfer curves of GIZO/AlO_x TFTs for different concentrations annealed with and without FUV irradiation and b) output curve for the TFT with a concentration of 0.1 M without FUV irradiation at 250 ºC.

The effect of leakage current on the output curve was not observed for patterned devices, Figure 3.13 b), when compared with the output curve of TFT annealed at 350 ºC.

The use of FUV irradiation combined with the thermal annealing provides an additional energy which induces a degradation of volatile organic residues and a M–O–M network reorganization via efficient condensation and subsequent densification.[35] That irradiation worked better at a lower concentration because there is less organic to degrade resulting in a lower hysteresis, Figure 3.13 a), and in a thinner film confirmed by ellipsometry. For higher concentration the TFTs do not show significant influence of FUV on leakage current and lower I_G is mainly due to higher thickness. Consequently the dielectric solution with the lowest concentration was chosen to proceed to low temperatures. For this temperature the FUV lamp at a distance of 5 cm was not used because the temperature could damage the lamp.

Table 3.4 – Characteristic parameters of GIZO/AlO_x TFTs for different concentrations of dielectric annealed with and without FUV irradiation at 250 ºC

Concentration (M)	**Condition**	**W/L**	**Von** (V)	**I_{ON}/I_{OFF}**	**V_T** (V)	**S** (V/dec)	**μ_{SAT}** (cm^2/Vs)	**V_{Hyst}** (V)
0.1	250 ºC	10	-0.30	8.3×10^4	0.15	0.10	9.63	0.02
	250 ºC + FUV	10	-0.36	5.6×10^4	0.18	0.12	11.76	0.03
0.25	250 ºC	1	-0.14	1.2×10^4	0.37	0.15	31.67	0.18
	250 ºC + FUV	1	-0.05	9.7×10^3	0.29	0.13	34.30	0.14

3.4.3 Effect of FUV exposure parameters for low temperature annealing

TFTs were produced at 200 ºC, 180 ºC and 150 ºC in order to have compatibility with flexible substrates. For those temperatures a thermal annealing of dielectric film with and without FUV irradiation assistance were performed. In the case of using FUV irradiation were changed the lamp distances from the heating plate and time of annealing. The main contribution of the use of FUV irradiation in the performance of devices is the reduction of leakage current (I_G) by the elimination of the organic residue present in dielectric, as shown in Figure 3.14 a) and b), which is more effective when reducing the distance of the lamp to 5 cm.

Figure 3.14 shows the transfer curves a) and b) of TFTs at 200 ºC and 150 ºC, respectively for different annealing conditions using FUV irradiation or not, and the output curves c),d) for the devices with FUV irradiation for a lamp distance of 5 cm for 30 min. By reducing the annealing temperature of dielectric the hysteresis in the TFTs increases independently of the conditions used (Table 3.5). The TFTs produced at 150 ºC have lower On/Off ratios, a worse quality in the interface between the dielectric-semiconductor and output curve, Figure 3.14 b) and d), when compared with devices at 200 ºC and 180 ºC in Table 3.5. These problems may be due to the fact of not achieving the temperature required to cause the combustion reaction, resulting only in solvent evaporation, as indicated in Figure 3.1 a).

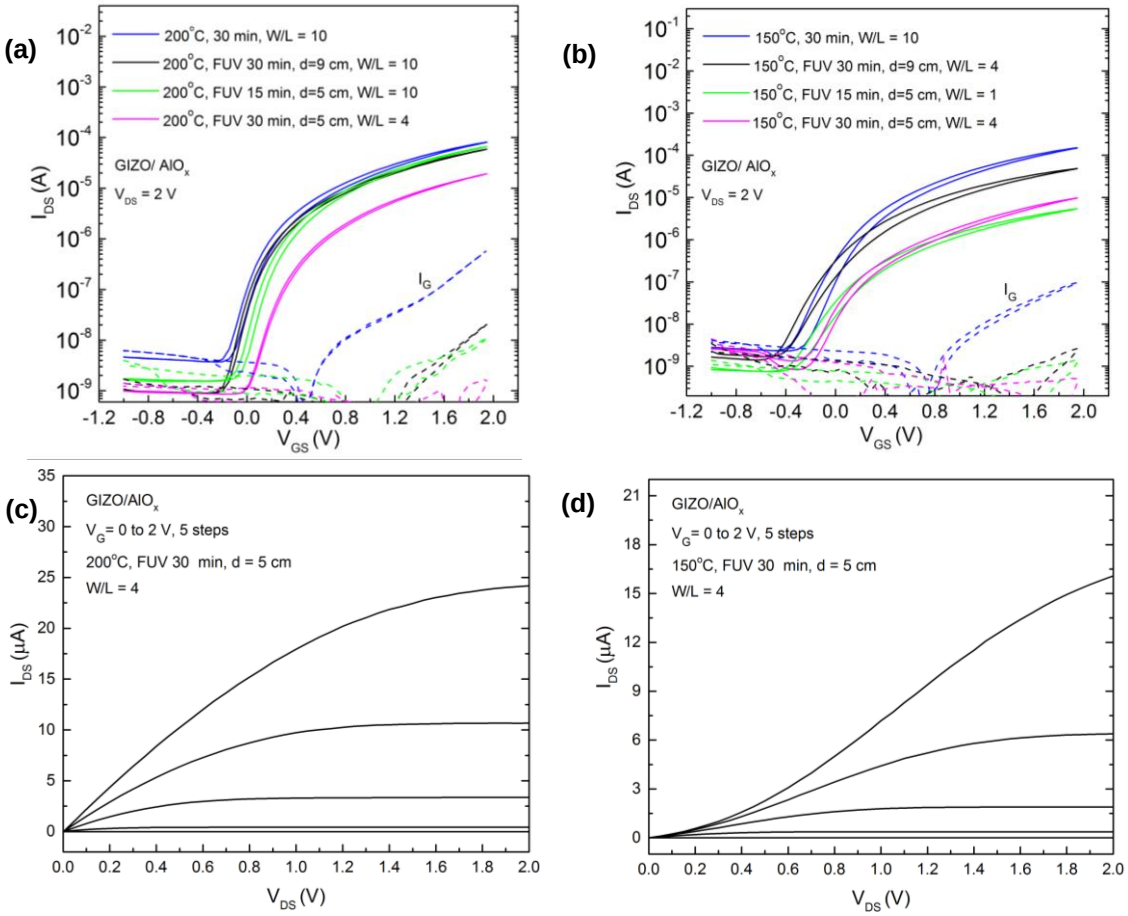

Figure 3.14 – Transfer curves of GIZO/AlO_x TFTs annealed at a) 200 ºC and b) 150 ºC for different annealing conditions and b) output curves for the TFTs with FUV irradiation combined with annealing for 30 min, c) and d), respectively.

So the temperature chosen to analyse the different conditions in further detail was 180 ºC because does not differ much of the characteristics parameters obtained for 200 ºC, Table 3.5, and is still compatible with flexible substrates.

Figure 3.15 a) shows the transfer curves of TFTs at 180 ºC in different conditions of annealing. By introducing FUV irradiation in the process of annealing the leakage current and hysteresis decrease, which is due to densification of the film, as seen in Table 3.5. Also, reducing the FUV lamp distance from 9 cm to 5 cm, decreases the leakage current almost an order of magnitude (Figure 3.15 a)), but the characteristic parameters remain very similar. After knowing that the leakage current was lower for a distance of 5 cm, due to irradiation being more efficient the annealing time was reduced to be more compatible with R2R process. As a result the On/Off ratio decreases slightly and threshold voltage (V_T), subthreshold slope (S) and hysteresis (V_{Hyst}) increase as can be seen in Table 3.5. Mobility is higher but that is an effect of the fringing electric field of using small channel ratio that leads to significantly overestimated field-effect mobility.[57] Taking this into account the best condition to use on TFTs with this dielectric is a combination of FUV irradiation, for a distance of 5 cm, with an annealing at 180ºC for 30 min. Figure 3.15 b) shows the output curve of TFT produced under these conditions.

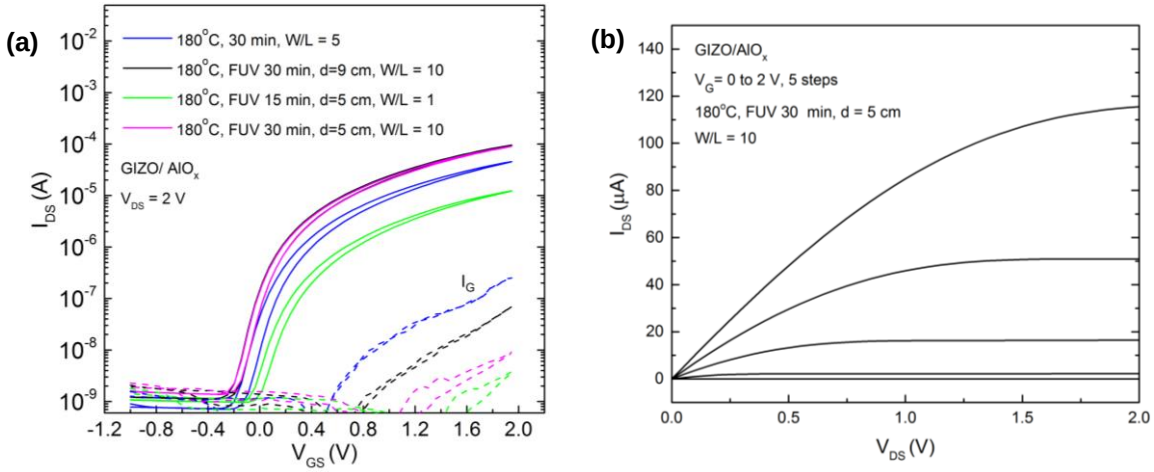

Figure 3.15 – a) Transfer curves of GIZO/AlO$_x$ TFTs for different annealing conditions and b) output curve for the TFT with FUV irradiation combined with annealing for 30 min at 180 ºC.

To study the uniformity and reproducibility of these devices, a set of 22 GIZO/AlO$_x$ TFTs was processed in identical conditions, 180 ºC annealing with FUV irradiation for 30 min, and characterized. These presented an average of saturation mobility (μ_{sat}) of 17.32 ± 4.15 cm^2/Vs, a subthreshold slope (S) of 0.11 ± 0.01 V/dec, a turn-on voltage (V_{on}) of -0.12 ± 0.06 V, a threshold voltage (V_T) of 0.13 ± 0.04 V, a hysteresis (V_{Hyst}) of 0.06 ± 0.02 V and an On/Off ratio of 5.30×10^4 ± 2.72×10^4 depicted on Annex K.

Table 3.5 – Electrical properties obtained for the devices depicted in Figure 3.14 a),b) and Figure 3.15 a).

Condition	Time (min)	Distance (cm)	$\frac{W}{L}$	Von (V)	I_{ON}/I_{OFF}	V_T (V)	S (V/dec)	μ_{SAT} (cm^2/Vs)	V_{Hyst} (V)
200 ºC	30	-	10	-0.25	2.20×10^4	0.16	0.12	13.47	0.05
200 ºC + FUV	30	9	10	-0.30	6.69×10^4	0.14	0.10	11.92	0.03
	30	5	4	-0.14	2.25×10^4	0.22	0.13	12.89	0.03
	15	5	10	-0.41	5.88×10^4	0.18	0.11	13.65	0.05
180 ºC	30	-	5	-0.25	6.46×10^4	0.19	0.11	17.05	0.08
180 ºC + FUV	30	9	10	-0.36	8.55×10^4	0.14	0.10	19.24	0.05
	30	5	10	-0.30	6.67×10^4	0.07	0.10	16.02	0.05
	15	5	1	-0.14	1.28×10^4	0.17	0.13	25.81	0.07
150 ºC	30	-	10	-0.41	6.54×10^4	0.28	0.15	32.86	0.12
150 ºC + FUV	30	9	4	-0.57	2.89×10^4	0.21	0.18	16.68	0.12
	30	5	4	-0.30	1.20×10^4	0.16	0.17	6.66	0.06
	15	5	1	-0.52	7.31×10^3	0.18	0.23	11.50	0.08

3.4.4 Stress measurements of optimized GIZO/AlO$_x$ TFTs

For the best production condition stress tests in GIZO/AlO$_x$ TFTs were performed in order to know if the devices were stable. Gate bias stress tests were performed in vacuum conditions (10^{-3} mbar, leaving the device at this pressure for 1 h prior starting the stress experiment) on these devices by applying a constant gate voltage equivalent to a 0.8 MV cm^{-1} electric field while maintaining source and drain electrodes grounded. The devices were stressed for 2 h, after which these were allowed to recover in the dark. Transfer characteristics were obtained in saturation regime, with a V_{DS} = 2 V at selected times during stress and recovery processes. Positive gate-bias stress (PBS) displaces the transfer curves to the negative direction (Annex L). Figure 3.16 shows the variation of V_T and S with the time during stress and recovery phases.

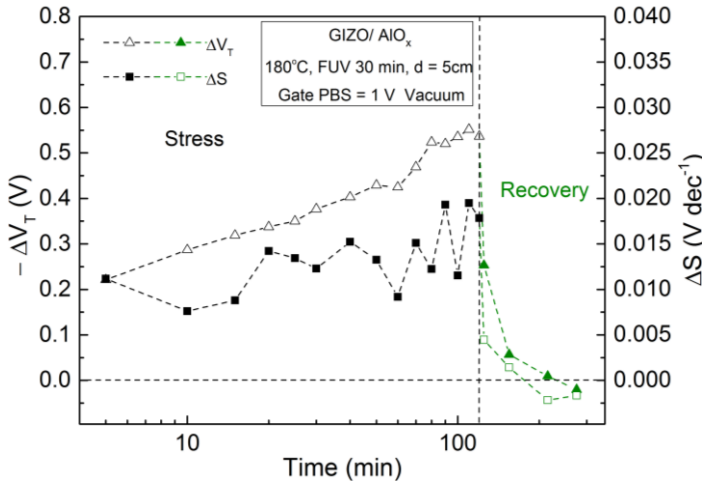

Figure 3.16 – Results obtained for a constant V_{GS} stress measurements on GIZO/AlO_x TFTs annealed at 180 ºC with FUV irradiation: Threshold voltage variation (ΔV_T) and subthreshold slope variation (ΔS) with the time during a 0.8 MV/cm a positive gate bias stress test at vacuum.

A negative V_T shift is observed when the device is subjected to a positive bias stress, with a V_{GS}= 1 V, and the value of subthreshold slope (S) does not change significantly during the course of stressing. In amorphous oxide TFTs, there are two possible reasons for the negative V_T shift, the ion migration within the gate dielectric [59] and charge trapping/detrapping in the gate dielectric causing instability in stress condition.[60], [61]. If ion drift were the reason for instability, after an extended period the device do not recover, because there is no driving force for ions to diffuse back to their original locations [59]. However, these devices show fast recovery of V_T when relaxed without the annealing treatment (Figure 3.16). Consequently the charge detrapping in the gate dielectric can be attributed to the observed negative shift under PBS process.

In contrary, the V_T shift under negative bias stress (NBS) shows smaller negative shift which is already reported for n-type semiconductor TFTs.[62] Figure 3.17 shows a negative V_T shift with little degradation of S. Humidity has a large impact in the negative shift of threshold voltage under NBS. So the device does not recover back very fast which is suggesting that the negative shift is due to the surface conduction in air (Annex L). Passivation or encapsulation of the TFT channel can improve stability.

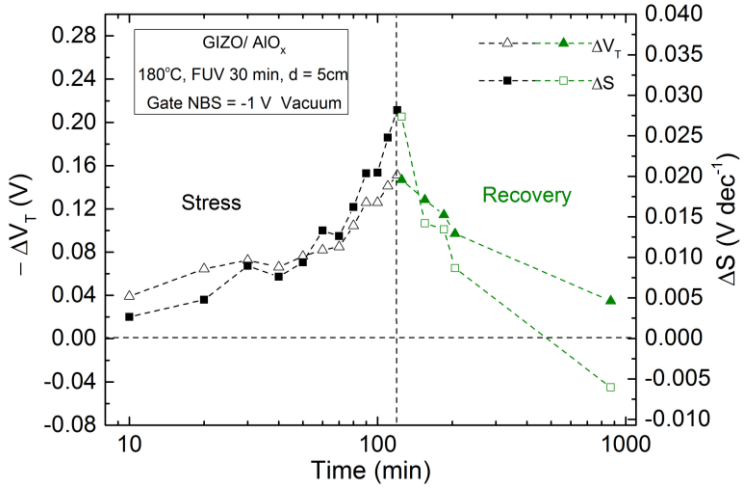

Figure 3.17 – Results obtained for a constant V_G stress measurements on GIZO/AlO_x TFTs annealed at 180 ºC with FUV irradiation: ΔV_T and ΔS with time during a 0.8 MV/cm a negative gate bias stress test at vacuum.

3.4.5 Stability over time of optimized GIZO/AlO$_x$ TFTs

Optimized TFTs were produced at low temperatures with different times of annealing combined with FUV irradiation with a lamp distance of 5 cm. To know how TFTs behaved over time measurements after 6 and 9 weeks were done, Figure 3.18.

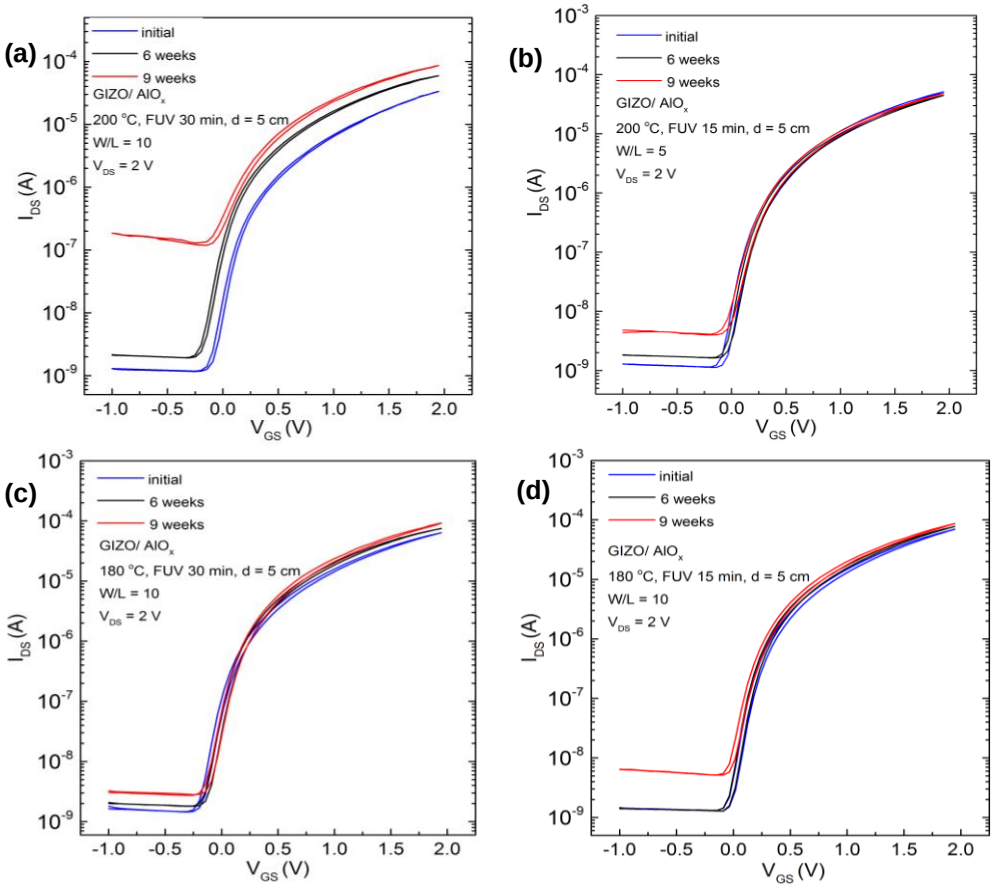

Figure 3.18 – Aging effects of GIZO/AlO$_x$ TFTs with different annealing conditions: Annealed at 200 ºC ((a) and (b)) and 180 ºC ((c) and (d)) with FUV irradiation for 30 and 15 min.

For 200 ºC the devices presented good stability after 6 weeks showing only a slight decrease in On/Off ratio, depicted in Figure 3.18 a),b). After 9 weeks the TFT subjected to 30 min of annealing at 200 ºC had an abrupt reduction of two orders of magnitude of On/Off ratio, Figure 3.18 a), and showed a decrease in the quality of the interface between the semiconductor and dielectric associated with an increasing of subthreshold slope (S).

Table 3.6 – Electrical properties obtained for the devices depicted in Figure 3.18.

Condition	Time (min)	Measure	W/L	Von (V)	I_{ON}/I_{OFF}	V_T (V)	S (V/dec)	μ_{SAT} (cm^2/Vs)	V_{Hyst} (V)
200 ºC + FUV d = 5cm	30	initial	10	-0.25	2.85×10^4	0.15	0.11	10.64	0.03
		6 weeks		-0.30	3.10×10^4	0.07	0.11	10.87	0.03
		9 weeks		-0.14	7.32×10^2	-0.03	0.25	15.29	0.04
	15	initial	5	-0.14	4.57×10^4	0.22	0.11	23.71	0.05
		6 weeks		-0.20	2.71×10^4	0.11	0.11	18.52	0.04
		9 weeks		-0.20	1.20×10^4	0.14	0.14	19.60	0.05
180 ºC + FUV d = 5 cm	30	initial	10	-0.30	4.39×10^4	0.13	0.11	11.15	0.04
		6 weeks		-0.25	4.18×10^4	0.03	0.10	13.28	0.04
		9 weeks		-0.25	3.26×10^4	0.06	0.11	16.79	0.04
	15	initial	10	-0.09	5.45×10^4	0.15	0.10	14.71	0.04
		6 weeks		-0.09	6.08×10^4	0.12	0.09	15.09	0.04
		9 weeks		-0.09	1.67×10^4	0.14	0.11	17.94	0.04

At 180 ºC the TFTs demonstrate improved stability (Table 3.6) showing only a higher decrease of On/Off ratio on TFT annealed for 15 min after 9 weeks, Figure 3.18 d), when compared with the TFT annealed for 30 min, Figure 3.18 c). For the lowest annealing temperature at 150 ºC a slight improvement of the devices occurred over time; turn-on voltage became closer to zero and the subthreshold slope decreased (Annex M).

In conclusion all devices operate at low voltages and are affected over time by humidity exposure of the environment due to the surface adsorption of water causing a decrease of On/Off ratio independently of the conditions used.[63] To solve this problem is necessary to passivate the devices.

3.4.6 Fully solution-based In_2O_3/AlO_x TFTs

Fully solution-based TFTs using a semiconductor present in literature [35] processed by solution, In_2O_3, were produced after know that dielectric have a good performance at low temperatures. For these devices the combination of FUV irradiation with thermal annealing at 200 ºC and 180 ºC, for 15 or 30 min was used on each constituent layer, dielectric and semiconductor. Figure 3.19 present the transfer curves of devices annealed at a) 200 ºC and b) 180 ºC, and their output curves for 30 min of annealing, Figure 3.19 c) and d), respectively.

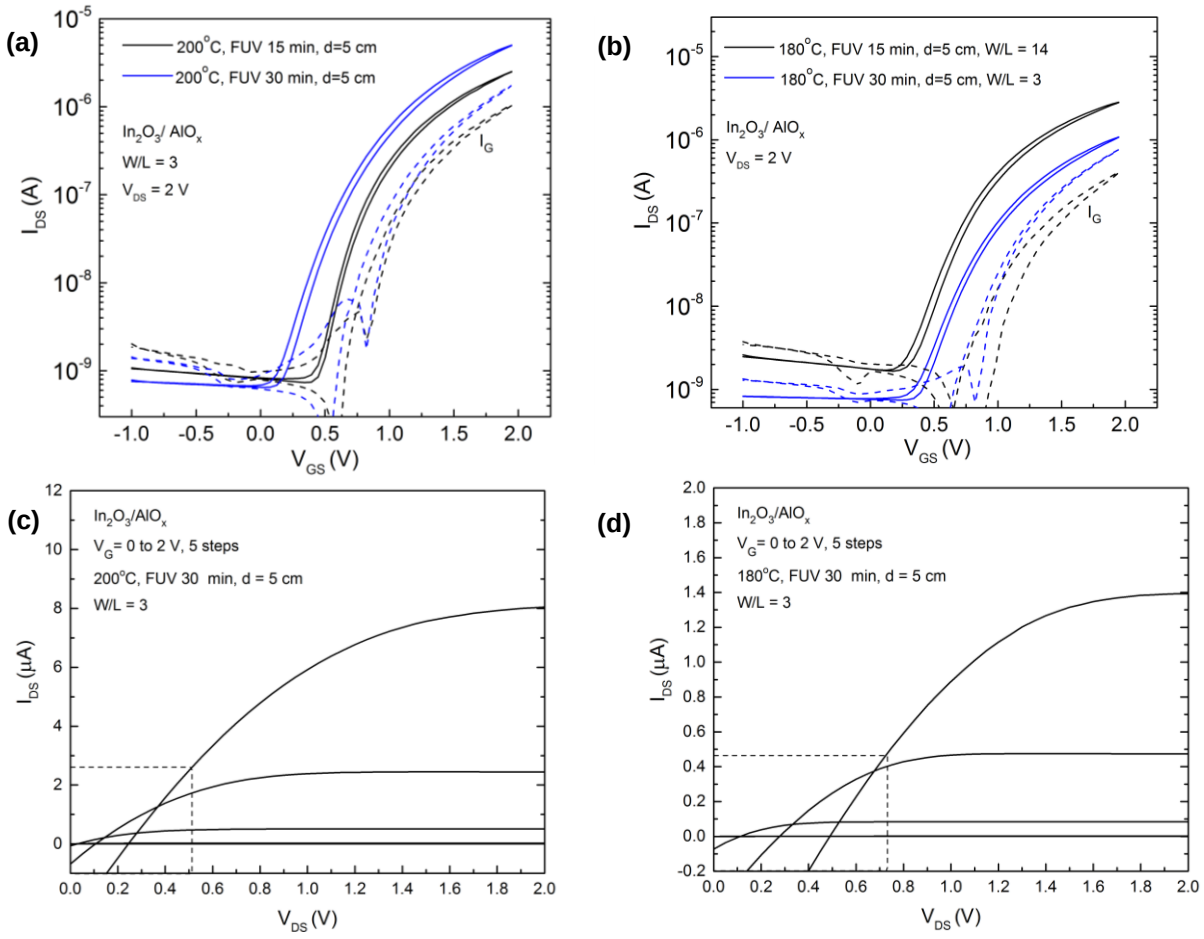

Figure 3.19 –Transfer curves of In_2O_3/AlO_x TFTs for different times of annealing with FUV at a) 200 ºC and c) 180 ºC. Output curves for the devices annealed for 30 min at c) 200 ºC and d) 180 ºC.

For 15 min of annealing of each layer all the devices showed a lower subthreshold slope (S) compared to 30 min, Figure 3.19. At 200 ºC TFTs showed a better performance: a higher saturation mobility of 5.57 cm^2/Vs, a better interface between semiconductor and dielectric, and a lower hysteresis when compared with TFTs produced at lower temperature as depicted in Table 3.7. Nonetheless these devices deteriorate over time , as shown in Figure 3.20 a),b), when

compared with TFTs annealed at 180 ºC that remain more stable, as presented in Figure 3.20 c),d).

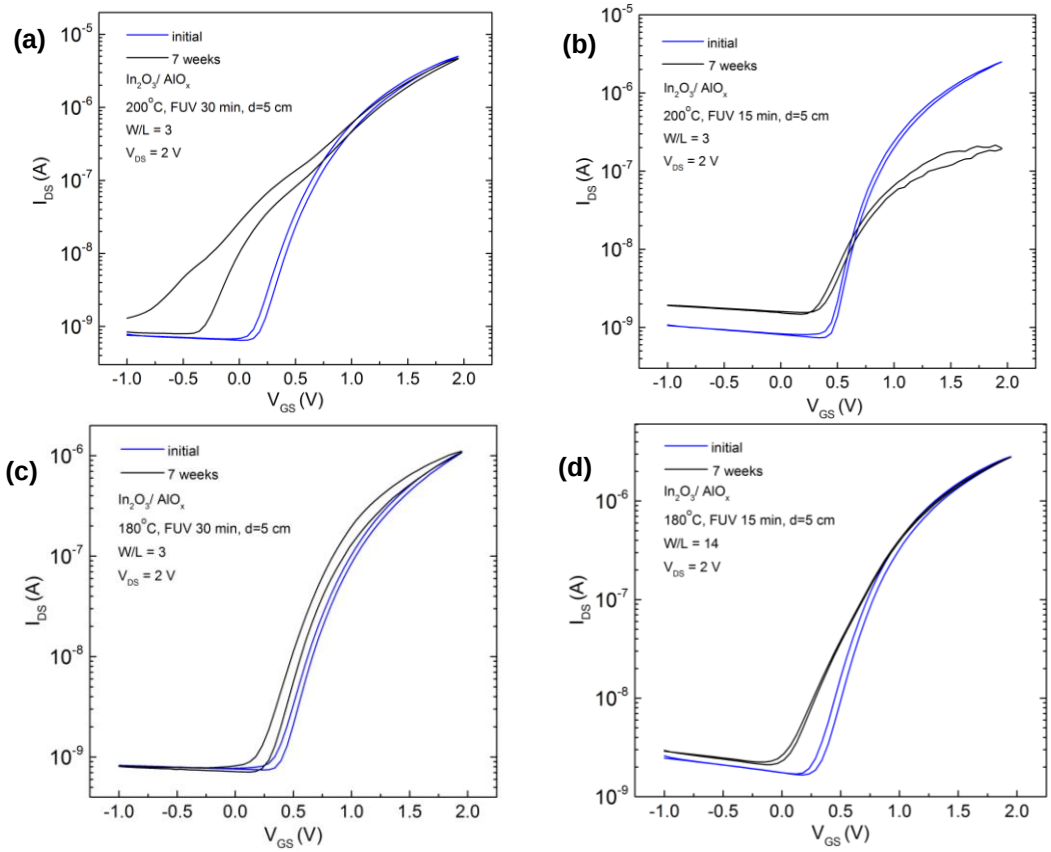

Figure 3.20 – Aging effects seen by the evolution of the transfer characteristics of In_2O_3/ AlO_x TFTs with different annealing methods: Annealed each layer at 200 ºC with FUV radiation for a) 30 and b) 15 min; Annealed each layer at 180 ºC with FUV radiation for c) 30 and d) 15 min.

The output curves illustrates the same behavior than for TFTs produced at 350 ºC (Figure 3.12 d)) where gate leakage current increase with positive V_{GS} for different temperatures, Figure 3.19 c) and d), which is due to non-patterned semiconductor with common gate, can be improved by patterning the semiconductor layer.

Table 3.7 – Electrical properties obtained for the devices depicted in Figure 3.19 a), b) and Figure 3.20.

Condition	Time (min)	Measure	W/L	Von (V)	I_{ON}/I_{OFF}	V_T (V)	S (V/dec)	μ_{SAT} (cm^2/Vs)	V_{Hyst} (V)
200 ºC + FUV	30	initial	3	0.02	7.76×10^3	0.51	0.20	5.57	0.06
		7 weeks		-0.52	5.80×10^3	0.57	0.28	5.57	0.57
	15	initial		0.34	3.40×10^3	0.57	0.15	3.02	0.04
		7 weeks		0.18	1.46×10^2	0.30	0.32	0.35	0.19
180 ºC + FUV	30	initial	3	0.23	1.45×10^3	0.53	0.24	1.26	0.07
		7 weeks		0.13	1.52×10^3	0.47	0.24	1.01	0.11
	15	initial	14	0.18	1.70×10^3	0.50	0.23	0.55	0.06
		7 weeks		-0.09	1.32×10^3	0.43	0.35	0.48	0.05

Taking into account the results obtained it was concluded that before measuring the devices over time the best condition was using an annealing at 200 ºC for 30 min, however TFTs annealed at 180 ºC for 30 min show improved stability over time.

3.4.7 Influence of DUV irradiation in GIZO/AlO$_x$ TFT

As deep ultraviolet (DUV) lamp have a lamp peak (253.7 nm) near to the dielectric solution absorption peak (245 nm) was tested the influence of DUV irradiation (lamp distance of 2 cm) in the dielectric film for 2 h in an ozone environment without annealing. However the GIZO semiconductor was annealed for one hour at 180 ºC subjecting the dielectric at that temperature. Figure 3.21 shows a) the transfer and b) output curves. The characteristic parameters presented were a subthreshold slope of 0.10 V/dec, a turn-on voltage of -0.30 V, a threshold voltage of 0.11 V, a hysteresis of 0.07 V, an On/Off ratio of 9.84×10^4 and a saturation mobility of 28.35 cm^2/Vs. This device showed good performance, low operating voltages, high On/Off ratio and higher saturation mobility than other devices that used the FUV irradiation lamp for the same temperature.

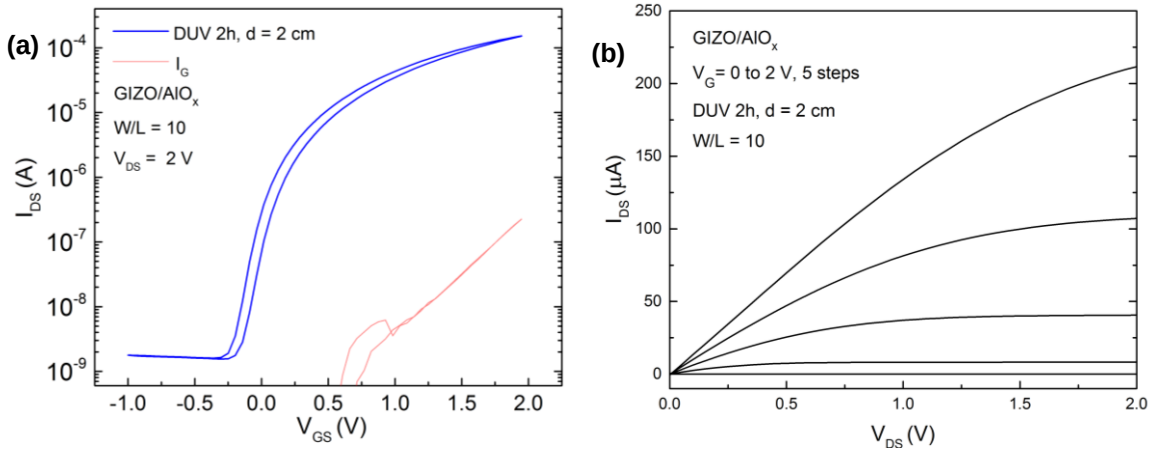

Figure 3.21 – a) Transfer and b) output curves of GIZO/AlO$_x$ TFT using DUV irradiation for 2 h in dielectric.

3.4.8 Flexible GIZO/AlO$_x$ TFT

As final step of this work, optimized GIZO/AlO$_x$ TFTs were produced at low temperatures with FUV irradiation on flexible PET substrates. The device was annealed at 200 ºC with FUV irradiation for 30 min, and the results are depicted in Figure 3.22. The device showed a saturation mobility of 7.66 cm^2/Vs, a V_{on} of -0.36 V, a V_T of -0.18 V, a subthreshold slope of 0.21 V/dec and an On/Off ratio of 1.40×10^3. Although performance is not as good as for devices in Si substrates, but the results are promising and process optimization should lead to further improvement.

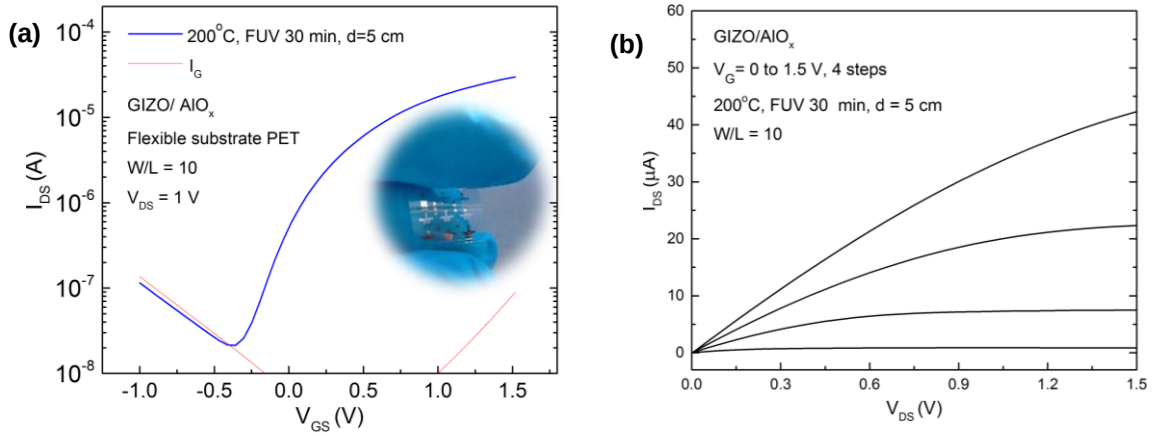

Figure 3.22 – a) Transfer and b) output curves of GIZO/AlO$_x$ TFTs with the dielectric annealed at 200 ºC combined with FUV irradiation in a PET substrate.

4. Conclusions and Future Perspectives

The work in this dissertation was focused on the study and optimization of the annealing processes of alumina dielectric processed by solution in order to have compatibility with flexible low cost substrates based on polymeric materials. After optimization the dielectric was applied in TFTs with different oxide semiconductors produced by solution and by sputtering in order to evaluate their performances.

First different aluminum oxide precursor solutions were studied. All of them absorbed in the UV region and the thin films of alumina showed an amorphous nature, transparency (91%) and good uniformity. MIS structures produced at 350 ºC with dielectric using aluminum nitrate precursor solution shows better results; lower hysteresis and higher stability when compared with chloride precursors. The use of fuel in reaction was required to provide additional heat in the combustion reaction in order to proceed for low temperatures as such two different fuels, citric acid and urea, were tested. Urea has a smaller molecule size resulting in a higher agglomeration of particles when the combustion reaction occurs, this leads to more uniform films and lower leakage current density. Therefore the best alumina precursor solution to proceed for low temperatures was aluminum nitrate and urea as fuel in 2-ME. The implementation of FUV irradiation at a lamp distance of 9 cm combined with thermal annealing at 250 ºC for a low concentration of 0.1 M reveals a significant improvement in leakage current and hysteresis because absorption of ultraviolet is more efficient and helps in densification, condensation and impurity decomposition of the thin film. For lower temperatures a lower distance to the FUV lamp was implemented being more efficient on densification of the films resulting in a low hysteresis and thickness when compared with just thermal annealing. Also, the time of annealing combined with FUV irradiation was reduced to make it more compatible with R2R. The ideal conditions for this dielectric were obtained using a lamp distance of 5 cm with an annealing time of 30 min.

After study the dielectric, different precursor solutions were applied in TFTs at 350 ºC for different semiconductors. Then the GIZO/AlO_x TFTs were chosen instead of ZTO/AlO_x TFTs to proceed for low temperatures because they had a lower hysteresis, a higher On/Off ratio and a better interface quality between dielectric and semiconductor. All the TFTs presented a higher leakage current due to non-patterning of semiconductors; knowing that all TFTs for lower temperatures were patterned. For low temperatures the devices depicted a good behavior and the temperature chosen to analyze in further detail was 180 ºC for 30 min assisted by FUV irradiation at a lamp distance of 5 cm. A study of uniformity and reproducibility of these devices was made where 22 TFTs presented a good performance with an average saturation mobility of 17.32 ± 4.51 cm^2/Vs, a subthreshold slope of 0.11 ± 0.01 V/dec, a turn-on voltage of -0.12 ± 0.06 V and a threshold voltage of 0.13 ± 0.04 V. These TFTs demonstrate the best stability over time showing only a small increase of Off current due to the exposure to the environment which can be solved with the passivation of devices.

The In_2O_3/AlO_x TFTs fully solution based are equivalent to the published ones and in some cases surpassing the actual state of the art (Annex N).

The GIZO/AlO_x TFT where the dielectric used DUV irradiation followed by thermal annealing at 180 ºC exhibited a better mobility when compared with the TFT exposed to the FUV irradiation, but have a higher leakage current.

In conclusion, all the TFTs that use lower temperatures operate at low voltages and can be applied in flexible substrates as seen for GIZO/AlO_x TFTs in a PET substrate using a thermal annealing of 200 ºC combined with FUV irradiation. However, the performance is not as good as for devices in Si substrates, but the results are promising and process optimization should lead to further improvement.

In this research work some questions and routes remain unknown and unanswered after this dissertation. Based on the results obtained here, some suggestions for future work are made:

- ✓ Increase the thickness of the dielectric slightly at low temperatures in order to decrease the leakage current that limit the Off current improving the On/Off ratio;
- ✓ Pattern the semiconductor of TFTs all based solution to decrease the leakage current;
- ✓ Passivate all the devices to avoid being affected by the environment over time;
- ✓ Study in further detail the use of DUV irradiation in dielectric but with thermal annealing for low temperatures;
- ✓ Use multilayers to improve the dielectric performance;
- ✓ Improve the behaviour of TFTs in flexible substrates by reducing the thickness of aluminum electrodes on gate of 100 nm to 40 nm because, as the dielectric is so thin, during the deposition the dielectric could not stay well dispersed in gate electrode. Another improvement is use phosphoric acid to remove the insulator from the top of gate electrode which can cause an increase in the On/Off ratio and reduce leakage current;
- ✓ The GIZO TFTs at low temperatures can be applied in basic building blocks, sensors and OLEDs (Figure 4.1).

Figure 4.1 – Flexible OLED display with TFT backplane (*Image property of TNO/Holst Centre, under the framework of the FP7 project ORAMA*).

5. References

[1] M.-G. Kim, M. G. Kanatzidis, A. Facchetti, and T. J. Marks, “Low-temperature fabrication of high-performance metal oxide thin-film electronics via combustion processing.,” *Nat. Mater.*, vol. 10, no. 5, pp. 382–8, May 2011.

[2] Y.-H. Kim, J.-S. Heo, T.-H. Kim, S. Park, M.-H. Yoon, J. Kim, M. S. Oh, G.-R. Yi, Y.-Y. Noh, and S. K. Park, “Flexible metal-oxide devices made by room-temperature photochemical activation of sol-gel films.,” *Nature*, vol. 489, no. 7414, pp. 128–32, Sep. 2012.

[3] C. Avis and J. Jang, “High-performance solution processed oxide TFT with aluminum oxide gate dielectric fabricated by a sol–gel method,” *J. Mater. Chem.*, vol. 21, no. 29, p. 10649, 2011.

[4] S.-Y. Han, G. S. Herman, and C. Chang, “Low-temperature, high-performance, solution-processed indium oxide thin-film transistors.,” *J. Am. Chem. Soc.*, vol. 133, no. 14, pp. 5166–9, Apr. 2011.

[5] X. Yu, J. Smith, N. Zhou, L. Zeng, P. Guo, Y. Xia, A. Alvarez, S. Aghion, H. Lin, J. Yu, R. P. H. Chang, M. J. Bedzyk, R. Ferragut, T. J. Marks, and A. Facchetti, “Spray-combustion synthesis: Efficient solution route to high-performance oxide transistors,” *Proc. Natl. Acad. Sci.*, vol. 112, no. 11, pp. 3217–3222, 2015.

[6] E. J. Bae, Y. H. Kang, M. Han, C. Lee, and S. Y. Cho, “Soluble oxide gate dielectrics prepared using the self-combustion reaction for high-performance thin-film transistors,” *J. Mater. Chem. C*, vol. 2, no. 28, p. 5695, 2014.

[7] H. Tan, G. Liu, A. Liu, B. Shin, and F. Shan, “The annealing effects on the properties of solution-processed alumina thin film and its application in TFTs,” *Ceram. Int.*, pp. 1–7, 2015.

[8] S. Dutta, A. Pandey, I. Yadav, O. P. Thakur, A. Kumar, R. Pal, and R. Chatterjee, “Growth and electrical properties of spin coated ultrathin ZrO2 films on silicon,” *J. Appl. Phys.*, vol. 114, no. 1, p. 014105, Jul. 2013.

[9] G. X. Liu, A. Liu, F. K. Shan, Y. Meng, B. C. Shin, E. Fortunato, and R. Martins, “High-performance fully amorphous bilayer metal-oxide thin film transistors using ultra-thin solution-processed ZrOx dielectric,” *Appl. Phys. Lett.*, vol. 105, no. 11, p. 113509, Sep. 2014.

[10] L. Xifeng, X. Enlong, and Z. Jianhua, “Low-Temperature Solution-Processed Zirconium Oxide Gate Insulators for Thin-Film Transistors,” *IEEE Trans. Electron Devices*, vol. 60, no. 10, pp. 3413–3416, Oct. 2013.

[11] G. D. Wilk, R. M. Wallace, and J. M. Anthony, “High-k gate dielectrics: Current status and materials properties considerations,” *J. Appl. Phys.*, vol. 89, no. 10, pp. 5243–5275, 2001.

[12] P. Barquinha, L. Pereira, G. Gonçalves, D. Kuscer, M. Kosec, A. Vilà, A. Olziersky, J. R. Morante, R. Martins, and E. Fortunato, “Low-temperature sputtered mixtures of high-κ and high bandgap dielectrics for GIZO TFTs,” *J. Soc. Inf. Disp.*, vol. 18, no. 10, p. 762, 2010.

[13] Y. M. Park, A. Desai, A. Salleo, and L. Jimison, “Solution-Processable Zirconium Oxide Gate Dielectrics for Flexible Organic Field Effect Transistors Operated at Low Voltages,” *Chem. Mater.*, vol. 25, no. 13, pp. 2571–2579, Jul. 2013.

[14] S. Y. Lee, S. Chang, and J.-S. Lee, “Role of high-k gate insulators for oxide thin film transistors,” *Thin Solid Films*, vol. 518, no. 11, pp. 3030–3032, Mar. 2010.

[15] R. Ponce Ortiz, A. Facchetti, and T. J. Marks, “High-k organic, inorganic, and hybrid dielectrics for low-voltage organic field-effect transistors.,” *Chem. Rev.*, vol. 110, no. 1, pp. 205–39, Jan. 2010.

[16] J. Robertson, “High dielectric constant oxides,” *Eur. Phys. J. Appl. Phys.*, vol. 28, no. 3, pp. 265–291, Dec. 2004.

[17] A. Sharma, O. P. Modi, and G. K. Gupta, “Effect of fuel to oxidizer ratio on synthesis of Alumina powder using Solution Combustion Technique-Aluminium Nitrate & Glycine combination,” vol. 3, no. 4, pp. 2151–2158, 2012.

[18] P. D. Ye, G. D. Wilk, B. Yang, J. Kwo, S. N. G. Chu, S. Nakahara, H. J. L. Gossmann, J. P. Mannaerts, M. Hong, K. K. Ng, and J. Bude, “GaAs metal-oxide-semiconductor field-effect transistor with nanometer-thin dielectric grown by atomic layer deposition,” *Appl. Phys. Lett.*, vol. 83, no. 1, pp. 180–182, 2003.

[19] T. Sekitani, U. Zschieschang, H. Klauk, and T. Someya, “Flexible organic transistors and circuits with extreme bending stability.,” *Nat. Mater.*, vol. 9, no. 12, pp. 1015–22, Dec. 2010.

[20] K. Yim, Y. Yong, J. Lee, K. Lee, H.-H. Nahm, J. Yoo, C. Lee, C. Seong Hwang, and S. Han, “Novel high-κ dielectrics for next-generation electronic devices screened by automated ab initio calculations,” *NPG Asia Mater.*, vol. 7, no. 6, p. e190, Jun. 2015.

[21] W. A. MacDonald, “Engineered films for display technologies,” *J. Mater. Chem.*, vol. 14, no. 1, p. 4, Dec. 2004.

[22] K. Nomura, H. Ohta, A. Takagi, T. Kamiya, M. Hirano, and H. Hosono, “Room-temperature fabrication of transparent flexible thin-film transistors using amorphous oxide semiconductors.,” *Nature*, vol. 432, no. 7016, pp. 488–92, Nov. 2004.

[23] K. Nomura, H. Ohta, K. Ueda, T. Kamiya, M. Hirano, and H. Hosono, “Thin-film transistor fabricated in single-crystalline transparent oxide semiconductor.,” *Science*, vol. 300, no. 5623, pp. 1269–72, May 2003.

[24] Y. Sun and J. A. Rogers, “Inorganic Semiconductors for Flexible Electronics,” *Adv. Mater.*, vol. 19, no. 15, pp. 1897–1916, Aug. 2007.

[25] A. G. Merzhanov, “The chemistry of self-propagating high-temperature synthesis,” *J. Mater. Chem.*, vol. 14, no. 12, p. 1779, Jun. 2004.

[26] R. K. Tukhtaev, V. V. Boldyrev, A. I. Gavrilov, S. V. Larionov, L. I. Myachina, and Z. A. Savel’eva, “Metal Sulfide Synthesis by Self-Propagating Combustion of Sulfur-Containing Complexes,” *Inorg. Mater.*, vol. 38, no. 10, pp. 985–991, 2002.

[27] H. C. Yi and J. J. Moore, “Self-propagating high-temperature (combustion) synthesis (SHS) of powder-compacted materials,” *J. Mater. Sci.*, vol. 25, no. 2, pp. 1159–1168, 1990.

[28] M. Epifani, E. Melissano, G. Pace, and M. Schioppa, “Precursors for the combustion synthesis of metal oxides from the sol–gel processing of metal complexes,” *J. Eur. Ceram. Soc.*, vol. 27, no. 1, pp. 115–123, Jan. 2007.

[29] H. J. Ha, S. W. Jeong, T.-Y. Oh, M. Kim, K. Choi, J. H. Park, and B.-K. Ju, “Flexible low-voltage pentacene memory thin-film transistors with combustion-processable Al 2 O 3 gate dielectric and Au nanoparticles,” *J. Phys. D. Appl. Phys.*, vol. 46, no. 23, p. 235102, Jun. 2013.

[30] T. Clark, J. D. Ruiz, H. Fan, C. J. Brinker, B. I. Swanson, and A. N. Parikh, “A New Application of UV−Ozone Treatment in the Preparation of Substrate-Supported, Mesoporous Thin Films,” *Chem. Mater.*, vol. 12, no. 12, pp. 3879–3884, Dec. 2000.

[31] H. Imai, A. Tominaga, H. Hirashima, M. Toki, and N. Asakuma, “Ultraviolet-reduced reduction and crystallization of indium oxide films,” *J. Appl. Phys.*, vol. 85, no. 1, p. 203, Jan. 1999.

[32] Y. M. Park, J. Daniel, M. Heeney, and A. Salleo, “Room-temperature fabrication of ultrathin oxide gate dielectrics for low-voltage operation of organic field-effect transistors.,” *Adv. Mater.*, vol. 23, no. 8, pp. 971–4, Feb. 2011.

[33] R. E. Van de Leest, “UV photo-annealing of thin sol-gel films,” *Appl. Surf. Sci.*, vol. 86, no. 1–4, pp. 278–285, Feb. 1995.

[34] S. Park, K.-H. Kim, J.-W. Jo, S. Sung, K.-T. Kim, W.-J. Lee, J. Kim, H. J. Kim, G.-R. Yi, Y.-H. Kim, M.-H. Yoon, and S. K. Park, “In-Depth Studies on Rapid Photochemical Activation of Various Sol-Gel Metal Oxide Films for Flexible Transparent Electronics,” *Adv. Funct. Mater.*, p. n/a–n/a, 2015.

[35] J. Leppäniemi, H. Majumdar, K. Ojanperä, T. Kololuoma, J. Dahl, M. Tuominen, P. Laukkanen, and A. Alastalo, “Rapid low-temperature processing of metal-oxide thin film transistors with combined far ultraviolet and thermal annealing,” *Appl. Phys. Lett.*, vol. 115, no. 11, pp. 1–10, 2014.

[36] David Halliday, Robert Resnick, and Jearl Walker, *Fundamentals of physics*, 9th ed. John Wiley & Sons, 2010.

[37] Cletus J. Kaiser, *The Capacitor Handbook*, 1st ed. New York: VAN NOSTRAND REINHOLD, 1993.

[38] “Wiley: Physics of Semiconductor Devices, 3rd Edition - Simon M. Sze, Kwok K. Ng,” 2006. [Online]. Available: http://eu.wiley.com/WileyCDA/WileyTitle/productCd-0471143235.html. [Accessed: 18-Jun-2015].

[39] A. Jakubowski and K. Iniewski, “Simple formulas for analysis of C-V characteristics of MIS capacitor,” *Solid. State. Electron.*, vol. 26, no. 8, pp. 755–756, Aug. 1983.

[40] K. Lehovec, “Analysis of C-V data in the accumulation regime of MIS structures,” *Solid. State. Electron.*, vol. 19, no. 12, pp. 993–996, Dec. 1976.

[41] E.H. Nicollian and J.R. Brews, *MOS (metal oxide semiconductor) physics and technology*. Wiley, 2002.

[42] J.-H. Lee, D. N.Liu, and S.-T. Wu, *Introduction to Flat Panel Displays*, 1st ed. John Wiley & Sons, Ltd, 2008.

[43] S. Wagner, H. Gleskova, I.-C. Cheng, and M. Wu, “Silicon for thin-film transistors,” *Thin Solid Films*, vol. 430, no. 1–2, pp. 15–19, 2003.

[44] C. R. Kagan and P. Andry, *Thin-Film Transistors*. New York: Marcel Dekker, Inc, 2003.

[45] A. C. Tickle, *Thin-film transistors: a new approach to microelectronics*. New York: John Wiley & Sons Inc, 1969.

[46] P. Barquinha, “PhD Thesis: Transparent Oxide Thin-Film Transistors : production, characterization and integration,” New University of Lisbon, 2010.

[47] P. Barquinha, L. Pereira, G. Gonçalves, R. Martins, and E. Fortunato, “Toward High-Performance Amorphous GIZO TFTs,” *J. Electrochem. Soc.*, vol. 156, no. 3, p. H161, 2009.

[48] R. Branquinho, D. Salgueiro, A. Santa, A. Kiazadeh, P. Barquinha, L. Pereira, R. Martins, and E. Fortunato, “Towards environmental friendly solution-based ZTO/AlO x TFTs,” *Semicond. Sci. Technol.*, vol. 30, no. 2, p. 024007, 2015.

[49] L. Pereira, H. Águas, E. Fortunato, and R. Martins, “Nanostructure characterization of high k materials by spectroscopic ellipsometry,” *Appl. Surf. Sci.*, vol. 253, no. 1, pp. 339–343, Oct. 2006.

[50] J. M. Reyes, B. M. Perez Ramos, C. Z. Islas, W. C. Arriaga, P. R. Quintero, and a. T. Jacome, “Chemical and Morphological Characteristics of ALD Al2O3 Thin-Film Surfaces after Immersion in pH Buffer Solutions,” *J. Electrochem. Soc.*, vol. 160, no. 10, pp. B201–B206, 2013.

[51] a. Dimoulas, G. Vellianitis, A. Travlos, V. Ioannou-Sougleridis, and A. G. Nassiopoulou, “Structural and electrical quality of the high-k dielectric Y[sub 2]O[sub 3] on Si (001): Dependence on growth parameters,” *J. Appl. Phys.*, vol. 92, no. 1, p. 426, 2002.

[52] C.-C. Hwang, T.-Y. Wu, J. Wan, and J.-S. Tsai, “Development of a novel combustion synthesis method for synthesizing of ceramic oxide powders,” *Mater. Sci. Eng. B*, vol. 111, no. 1, pp. 49–56, 2004.

[53] A. Rajaeiyan, “Comparison of Urea and Citric Acid Complexing Agents and Annealing Temperature Effect on the Structural Properties of γ- and α-Alumina Nanoparticles Synthesized by Sol-Gel Method,” vol. 2013, 2013.

[54] A. Chu, M. Qin, Rafi-Ud-Din, B. Jia, H. Lu, and X. Qu, “Citric acid-assisted combustion-carbothermal synthesis of well-distributed highly sinterable AlN nanopowders,” *J. Am. Ceram. Soc.*, vol. 95, no. 8, pp. 2510–2515, 2012.

[55] B. Du Ahn, H.-J. Jeon, J. Sheng, J. Park, and J.-S. Park, “A review on the recent developments of solution processes for oxide thin film transistors,” *Semicond. Sci. Technol.*, vol. 30, no. 6, p. 064001, 2015.

[56] C. Avis and J. Jang, “High-performance solution processed oxide TFT with aluminum oxide gate dielectric fabricated by a sol–gel method,” *J. Mater. Chem.*, vol. 21, no. 29, p. 10649, Jul. 2011.

[57] K. Okamura, D. Nikolova, N. Mechau, and H. Hahn, “Appropriate choice of channel ratio in thin-film transistors for the exact determination of field-effect mobility,” *Appl. Phys. Lett.*, vol. 94, no. 18, pp. 3–5, 2009.

[58] Y. S. Rim, H. S. Lim, and H. J. Kim, “Low-temperature metal-oxide thin-film transistors formed by directly photopatternable and combustible solution synthesis,” *ACS Appl. Mater. Interfaces*, vol. 5, no. 9, pp. 3565–3571, 2013.

[59] J. F. Wager, D. A. Keszler, and R. E. Presley, *Transparent Electronics*, 1 st. New York: Springer US, 2008.

[60] J. Lee, J.-S. Park, Y. S. Pyo, D. B. Lee, E. H. Kim, D. Stryakhilev, T. W. Kim, D. U. Jin, and Y.-G. Mo, “The influence of the gate dielectrics on threshold voltage instability in amorphous indium-gallium-zinc oxide thin film transistors,” *Appl. Phys. Lett.*, vol. 95, no. 12, p. 123502, Sep. 2009.

[61] Y. Vygranenko, K. Wang, and A. Nathan, “Stable indium oxide thin-film transistors with fast threshold voltage recovery,” *Appl. Phys. Lett.*, vol. 91, no. 26, p. 263508, Dec. 2007.

[62] J. F. Conley, “Instabilities in Amorphous Oxide Semiconductor Thin-Film Transistors,” *IEEE Trans. Device Mater. Reliab.*, vol. 10, no. 4, pp. 460–475, Dec. 2010.

[63] J. S. Park, J. K. Jeong, H. J. Chung, Y. G. Mo, and H. D. Kim, “Electronic transport properties of amorphous indium-gallium-zinc oxide semiconductor upon exposure to water,” *Appl. Phys. Lett.*, vol. 92, no. 7, pp. 34–36, 2008.

[64] S. L. González-Cortés and F. E. Imbert, “Fundamentals, properties and applications of solid catalysts prepared by solution combustion synthesis (SCS),” *Appl. Catal. A Gen.*, vol. 452, pp. 117–131, 2013.

[65] A. Sharma, O. P. Modi, and G. K. Gupta, “Combustion Synthesis of Nanocrystalline Al 2 O 3 Powder using Aluminium Nitrate and Urea as reactants—influence of reactant composition,” vol. 3, pp. 3819–3824, Jun. 2012.

[66] Z. Shao, W. Zhou, and Z. Zhu, “Advanced synthesis of materials for intermediate-temperature solid oxide fuel cells,” *Prog. Mater. Sci.*, vol. 57, no. 4, pp. 804–874, 2012.

[67] S. R. Jain, K. C. Adiga, and V. R. Pai Verneker, “A new approach to thermochemical calculations of condensed fuel-oxidizer mixtures,” *Combust. Flame*, vol. 40, pp. 71–79, Jan. 1981.

[68] Datasheet, “Hamamatsu Phothonics K.K.,” *H2D2 Light Source Unit L11798/-01*, no. mm. pp. 1–4.

[69] P. K. Nayak, M. N. Hedhili, D. Cha, and H. N. Alshareef, “High performance In2O3 thin film transistors using chemically derived aluminum oxide dielectric,” *Appl. Phys. Lett.*, vol. 103, no. 3, pp. 1–5, 2013.

[70] R. Branquinho, D. Salgueiro, L. Santos, P. Barquinha, L. Pereira, R. Martins, and E. Fortunato, “Aqueous combustion synthesis of aluminum oxide thin films and application as gate dielectric in GZTO solution-based TFTs.,” *ACS Appl. Mater. Interfaces*, vol. 6, no. 22, pp. 19592–9, Nov. 2014.

[71] J. Hwang, K. Lee, Y. Jeong, Y. U. Lee, C. Pearson, M. C. Petty, and H. Kim, “UV-Assisted Low Temperature Oxide Dielectric Films for TFT Applications,” *Adv. Mater. Interfaces*, p. n/a–n/a, Aug. 2014.

6. Annexes

Annex A

The synthesis of aluminum oxide with and without combustion using metal precursors and fuels in case of combustion, mentioned previously, follow the balance between aluminum nitrate decomposition reactions and the oxidation reaction of the fuels:[17], [51–53]

Table 6.1 – Reactions of reduction and oxidation.

Reduction reaction	
Aluminum nitrate nonahydrate	$2Al(NO_3)_3 \cdot 9H_2O \rightarrow Al_2O_3 + 18H_2O + 3N_2 + \left(\frac{15}{2}\right)O_2$
Ammonium nitrate	$NH_4NO_3 \rightarrow 2H_2O + N_2 + \left(\frac{1}{2}\right)O_2$
Aluminum Chloride hydrated + Ammonium nitrate	$2AlCl_3 \cdot 6H_2O + 4NH_4NO_3 \rightarrow Al_2O_3 + 20H_2O + 4N_2 + 3Cl_2 + \left(\frac{1}{2}\right)O_2$
Aluminum Chloride hydrated + Silver nitrate	$2AlCl_3 \cdot 6H_2O + 6AgNO_3 \rightarrow Al_2O_3 + 12H_2O + 6AgCl + \left(\frac{15}{2}\right)O_2 + 3N_2$
Oxidation reaction	
Urea	$CO(NH_2)_2 + \left(\frac{3}{2}\right)O_2 \rightarrow 2H_2O + CO_2 + N_2$
Citric acid	$C_6H_8O_7 + \left(\frac{9}{2}\right)O_2 \rightarrow 4H_2O + 6CO_2$
2-Methoxyethanol	$C_3H_8O_2 + 4O_2 \rightarrow 4H_2O + 3CO_2$

The reactions are given by the combination of reduction and oxidation reaction. In these combustion reactions occurs the formation of different gaseous products (H_2O, N_2, CO_2, O_2 and Cl_2) depending of the reaction.

Table 6.2 – Overall reaction given by the combination of reduction and oxidation reaction.

Precursor	Fuel	Overall reaction
Aluminum nitrate nonahydrate	Urea	$2Al(NO_3)_3 \cdot 9H_2O + CO(NH_2)_2 \rightarrow Al_2O_3 + 20H_2O + CO_2 + 4N_2 + 6O_2$
	Citric acid	$2Al(NO_3)_3 \cdot 9H_2O + C_6H_8O_7 \rightarrow Al_2O_3 + 22H_2O + 6CO_2 + 3N_2 + 3O_2$
	2-ME	$2Al(NO_3)_3 \cdot 9H_2O + C_3H_8O_2 \rightarrow Al_2O_3 + 22H_2O + 3CO_2 + 3N_2 + \left(\frac{7}{2}\right)O_2$
Aluminum Chloride hydrated + Ammonium nitrate	Urea	$2AlCl_3 \cdot 6H_2O + 4NH_4NO_3 + CO(NH_2)_2 \rightarrow Al_2O_3 + 22H_2O + CO_2 + 5N_2 + 3Cl_2 + O_2$
	Citric acid	$2AlCl_3 \cdot 6H_2O + 4NH_4NO_3 + C_6H_8O_7 \rightarrow Al_2O_3 + 24H_2O + 6CO_2 + 4N_2 + 3Cl_2 + 4O_2$
Aluminum Chloride hydrated + Silver nitrate	Urea	$2AlCl_3 \cdot 6H_2O + 6AgNO_3 + CO(NH_2)_2 \rightarrow Al_2O_3 + 14H_2O + 6AgCl + CO_2 + 4N_2 + 6O_2$
	Citric acid	$2AlCl_3 \cdot 6H_2O + 6AgNO_3 + C_6H_8O_7 \rightarrow Al_2O_3 + 16H_2O + 6AgCl + 6CO_2 + 3N_2 + 3O_2$

To ensure the redox stoichiometry of the reaction, using the relationship between redox stoichiometry and the molar ratio of the reactants, it is necessary to determine the valency of the reducing / oxidizing reagent (RV:OV):[67]

$$\varphi = \frac{RV}{OV} n \Leftrightarrow n = 1 \times \frac{OV}{RV} \quad (1.12)$$

Where n (Table 6.5) is the number of moles of fuel per mole of oxidant.

The ideal stoichiometric composition of redox mixture is obtained when is not necessary any molecular oxygen for the reaction being complete (φ = 1). When φ <1 the redox mixture is under a regime in poor fuel resulting in the production of molecular oxygen. On the other hand, if φ> 1 the redox mixture is under fuel-rich condition, requiring molecular oxygen to fully convert the fuel. In order to get φ =1, we have to calculate the oxidizing/reducing valences of a redox mixture. Metals, carbon and hydrogen are considered as reducing elements with the corresponding metal valence, +3 for aluminum, +4 for carbon and +1 for hydrogen. Oxygen is seen as an oxidizer with the valence −2 and nitrogen is considered with valence 0.[64]

Table 6.3 – Valence of all reagents

Reagents	Chemical formula	Calculation	Total
Oxidizing reagent (OV)	$Al(NO_3)_3$*	3 + (3 × 0) + (3 × 3 × -2)	-15
	NH_4NO_3	(1 × 0) + (1 × 4) + (1 × 0) + (3 × -2)	-2
Reducing reagent (RV)	$CO(NH_2)_2$	4 -2 + (2 × 0) + (2 × 2 × 1)	+6
	$C_3H_8O_2$	(3 × 4) + (1 × 8) + (2 × -2)	+16
	$C_6H_8O_7$	(6 × 4) + (8 × 1) + (7 × -2)	+18

*Hydration water does not affect the overall compound valence

Therefore it is possible to know the number of moles needed to ensure stoichiometry of the redox reaction. Now we can rewrite all the global reactions.[51, 54]

Table 6.4 – Number of moles (n) to ensure stoichiometry of the redox reaction.

Precursor	φ	Fuel	n
Aluminum nitrate nonahydrate	1	Urea	$\left(\frac{5}{2}\right)$
		Citric acid	$\left(\frac{5}{6}\right)$
Aluminum Chloride hydrated + Ammonium nitrate	1	Urea	1
		Citric acid	$\left(\frac{1}{3}\right)$
Aluminum Chloride hydrated + Silver nitrate	1	Urea	$\left(\frac{5}{2}\right)$
		Citric acid	$\left(\frac{5}{6}\right)$

Table 6.5 – Overall reaction with the correct stoichiometry.

Precursor	Fuel	Overall reaction
Aluminum nitrate nonahydrate	Urea	$2Al(NO_3)_3 + 5CO(NH_2)_2 \rightarrow Al_2O_3 + 10H_2O + 5CO_2 + 8N_2$
	Citric acid	$2Al(NO_3)_3 + \left(\frac{5}{3}\right) C_6H_8O_7 \rightarrow Al_2O_3 + \left(\frac{20}{3}\right) H_2O + 10CO_2 + 3N_2$
Aluminum Chloride hydrated + Ammonium nitrate	Urea	$2AlCl_3 + 6NH_4NO_3 + 2CO(NH_2)_2 \rightarrow Al_2O_3 + 13H_2O + 2CO_2 + 8N_2 + 6HCl$
	Citric acid	$2AlCl_3 + 6NH_4NO_3 + \left(\frac{2}{3}\right) C_6H_8O_7 + \left(\frac{1}{3}\right) O_2 \rightarrow Al_2O_3 + 12H_2O + 4CO_2 + 6N_2 + 6HCl$
Aluminum Chloride hydrated + Silver nitrate	Urea	$2AlCl_3 + 6AgNO_3 + 5CO(NH_2)_2 \rightarrow Al_2O_3 + 6AgCl + 5CO_2 + 8N_2 + 10H_2O$
	Citric acid	$2AlCl_3 + 6AgNO_3 + \left(\frac{5}{3}\right) C_6H_8O_7 \rightarrow Al_2O_3 + 6AgCl + \left(\frac{20}{3}\right) H_2O + 10CO_2 + 3N_2$

Annex B

Normalized spectral distribution of the FUV lamp used in dielectric and In_2O_3 films.

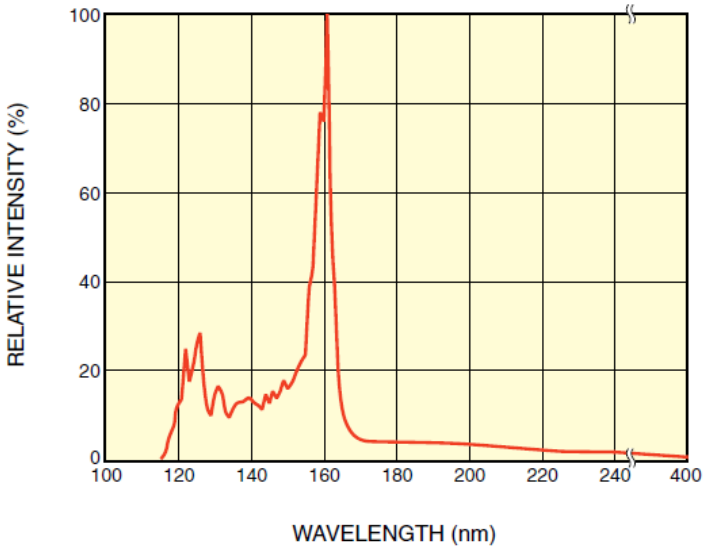

Figure 6.1 – Normalized spectral distribution of the FUV lamp (*Hamamatsu Phothonics)* with a higher incidence at a wavelength of 160 nm.[68]

Annex C

Thickness, capacitance and dielectric constant of all dielectric thin films produced.

Table 6.6 – Thickness of all the AlO_x thin films produced for different temperatures with different processing conditions in 2-ME for a frequency of 100 kHz.

Temperature (ºC)	Solution	Conditions	Thickness (nm)	Capacitance (nF/cm²)	Dielectric constant (k)
350	$Al(NO_3)_3$	t_A=30 min c=0.1 M	10.64	535	6.43
	$Al(NO_3)_3$ U		10.91	396	4.88
	$Al(NO_3)_3$ CA		12.16	281	3.87
	$AlCl_3$		20.52	328	7.52
	$AlCl_3$ NA U		11.63	407	5.35
	$AlCl_3$ NA CA		13.07	326	4.81
	$AlCl_3$ SN U		10.58	494	5.91
	$AlCl_3$ SN CA		13.37	432	6.52
250	$Al(NO_3)_3$ U	c=0.1 M, t_A=30 min	12.10	458	6.27
		c=0.1 M, t_A=30 min with FUV, d =9 cm	10.20	452	5.21
		c=0.25 M, t_A=30 min	30.15	292	9.93
		c=0.25 M, t_A=30 min with FUV, d =9 cm	30.40	185	6.34
200	$Al(NO_3)_3$ U	c=0.1 M, t_A=30 min	12.03	409	5.56
		c=0.1 M, t_A=30 min with FUV, d =9 cm	13.36	335	5.06
		c=0.1 M, t_A=30 min with FUV, d =5 cm	11.51	349	4.54
		c=0.1 M, t_A=15 min with FUV, d =5 cm	12.07	354	4.83
180	$Al(NO_3)_3$ U	c=0.1 M, t_A=30 min	13.98	438	6.92
		c=0.1 M, t_A=30 min with FUV, d =9 cm	12.67	336	4.81
		c=0.1 M, t_A=30 min with FUV, d =5 cm	11.87	381	5.11
		c=0.1 M, t_A=15 min with FUV, d =5 cm	11.58	381	4.98
		c=0.1 M, t_A=30 min, DUV 2h, d =2 cm	14.97	334	5.64
150	$Al(NO_3)_3$ U	c=0.1 M, t_A=30 min	15.36	376	6.52
		c=0.1 M, t_A=30 min with FUV, d =9 cm	11.65	401	5.28
		c=0.1 M, t_A=30 min with FUV, d =5 cm	12.05	334	4.54
		c=0.1 M, t_A=15 min with FUV, d =5 cm	12.04	358	4.87

Images obtained by the optical microscope for different precursor solutions.

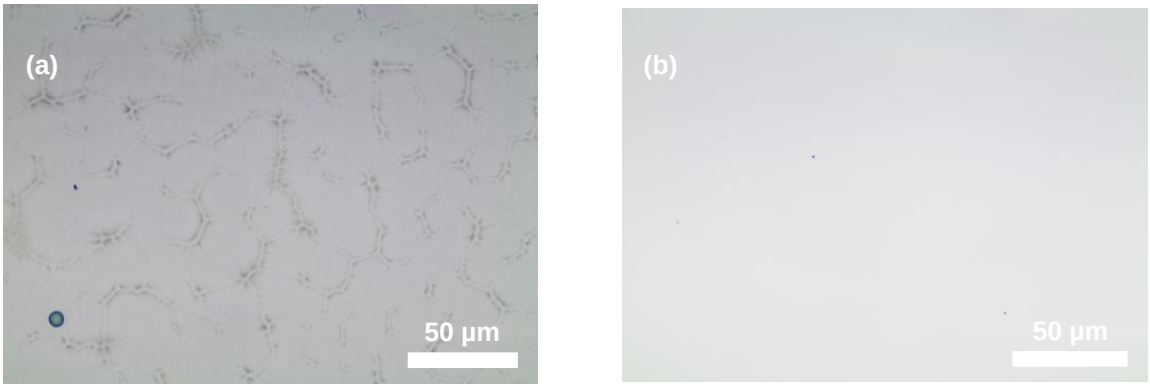

Figure 6.2 – Images at optical microscope of AlO_x thin films in Si at 350 ºC with a) aluminum chloride and b) aluminum nitrate as precursor solution in 2-ME.

Annex D

Transmittance spectra for AlO_x thin films in a glass substrate for different process conditions.

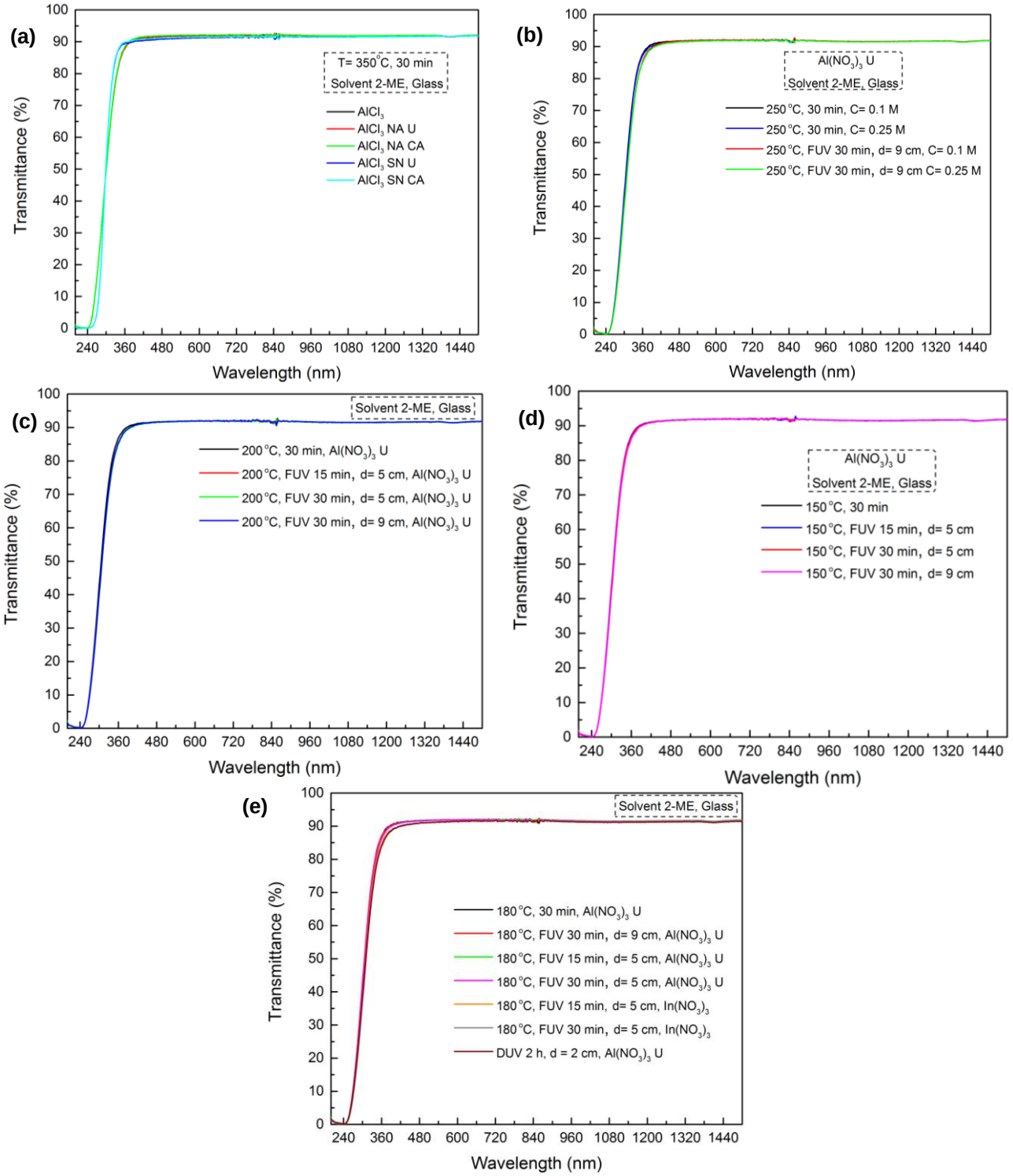

Figure 6.3 – Transmittance of thin films with different process conditions in glass: a) Thin films of aluminum chloride precursors with ammonium nitrate or silver nitrate using fuels (urea or citric acid) and without at 350 ºC. Thin films of aluminum nitrate using urea as fuel without and with FUV radiation: b) for different concentrations at 350 ºC; c) and d) for different distances of the lamp and time of annealing at 200 ºC and 150 ºC, respectively; e) Thin films of semiconductor and dielectric without and with FUV or DUV radiation for different process conditions at 180 ºC.

Annex E

FTIR (ATR) spectra of AlO_x thin films to identify the presence of their elements for different process conditions on a Si substrate.

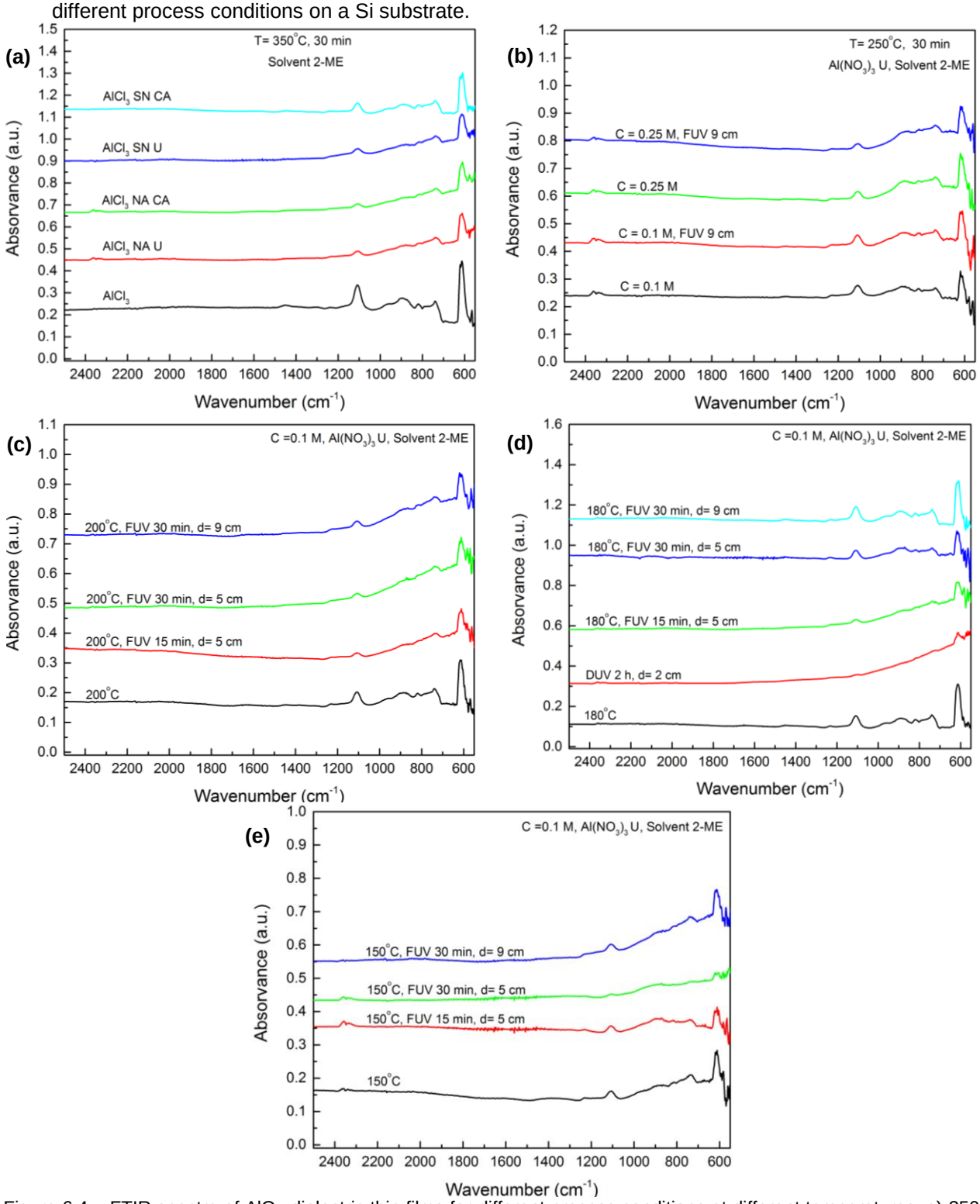

Figure 6.4 – FTIR spectra of AlOx dielectric thin films for different process conditions at different temperatures: a) 350 ºC, b) 250 ºC, c) 200 ºC, d) 180 ºC and e) 150 ºC.

Annex F

XRD of AlO_x thin films produced from aluminum nitrate using urea as fuel in 2-ME deposited on a Si substrate for different process conditions.

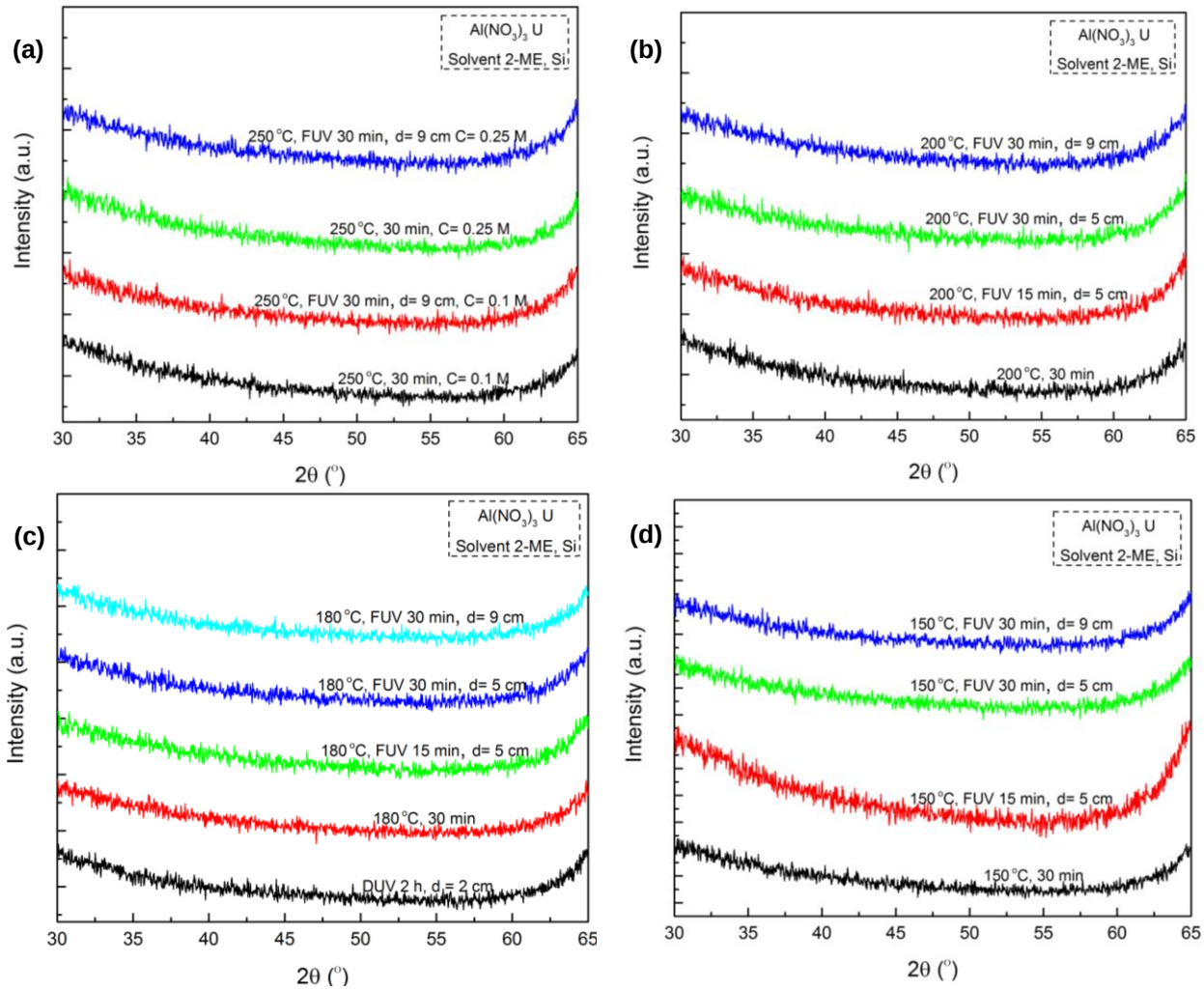

Figure 6.5 – XRD diffractograms of AlO_x dielectric thin film deposited on Si for different process conditions: a) Annealing the thin film at 250 ºC combined or not with FUV radiation for different concentrations, 0.1 M and 0.25 M; Thin films annealed at b) 200 ºC or c) 150 ºC without FUV assistance and with using different distances of the lamp for different times of annealing.; d) Thin films annealed at 180 ºC without FUV assistance and with using different distances of the lamp for different times of annealing and a film exposed to radiation DUV for 2 h.

Annex G

Surface morphology study of the dielectric (AlO_x) thin film with and without FUV irradiation by AFM.

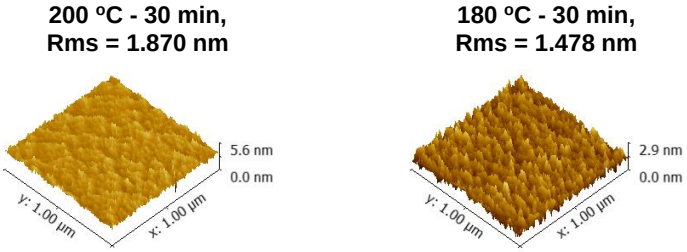

Figure 6.6 – Morphological characterization of 2-methoxyethanol (2-ME) solution based AlO_x ($Al(NO_3)_3$ with urea) thin films for different annealing temperatures.

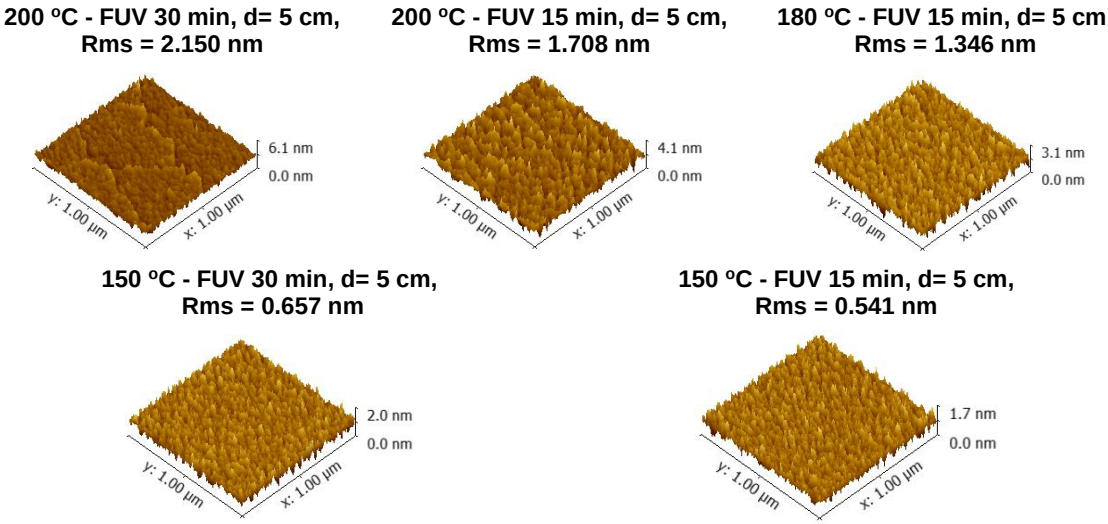

Figure 6.7 – Morphological characterization of 2-methoxyethanol (2-ME) solution based AlO_x ($Al(NO_3)_3$ with urea) thin films for different annealing temperatures and times combined with FUV irradiation (lamp distance of 5 cm).

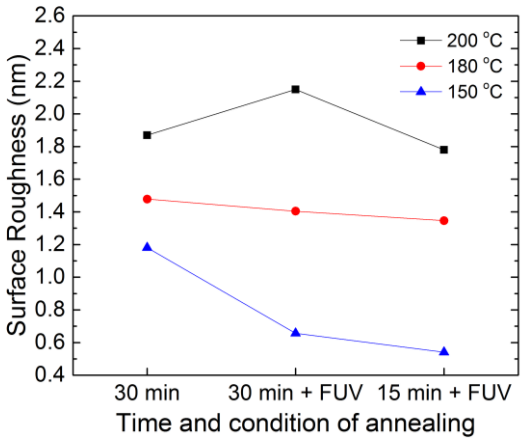

Figure 6.8 – AlO_x thin films surface roughness variation for different conditions of annealing.

For higher annealing temperatures the surface roughness of dielectric is higher and with the combination of lower annealing time and FUV irradiation is obtained less roughness (Figure 6.8).

Surface morphology study of the dielectric (AlO_x) thin film and the semiconductor (In_2O_3) deposited onto AlO_x thin films by SEM.

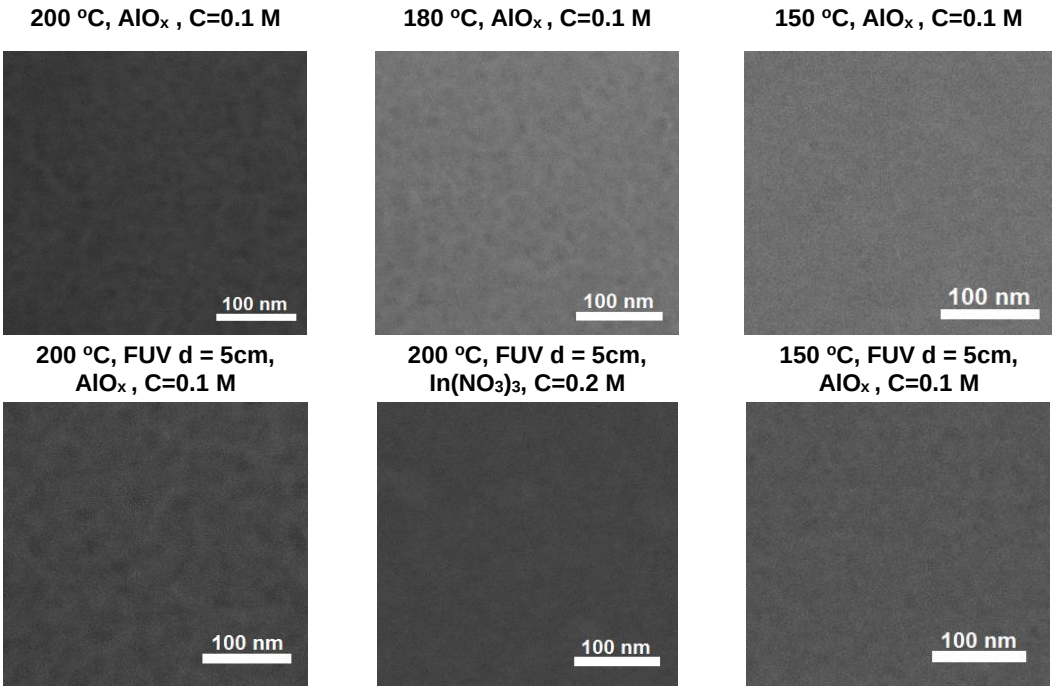

Figure 6.9 – Surface morphology of AlO_x ($Al(NO_3)_3$ with U in 2-ME) thin films using different methods of anneling for 30 min and 2-ME solution based In_2O_3 deposited onto AlO_x thin film annealed over 30 min at 200 ºC combined with FUV radiation.

Annex H

Electrical characterization of AlO_x MIS devices produced from $AlCl_3$ (Figure 6.10) and $Al(NO_3)_3$ using urea as fuel (Figure 6.11, Figure 6.12 and Figure 6.13) by capacity-voltage (CV), capacity-frequency (Cf) and current-voltage (IV) curves.

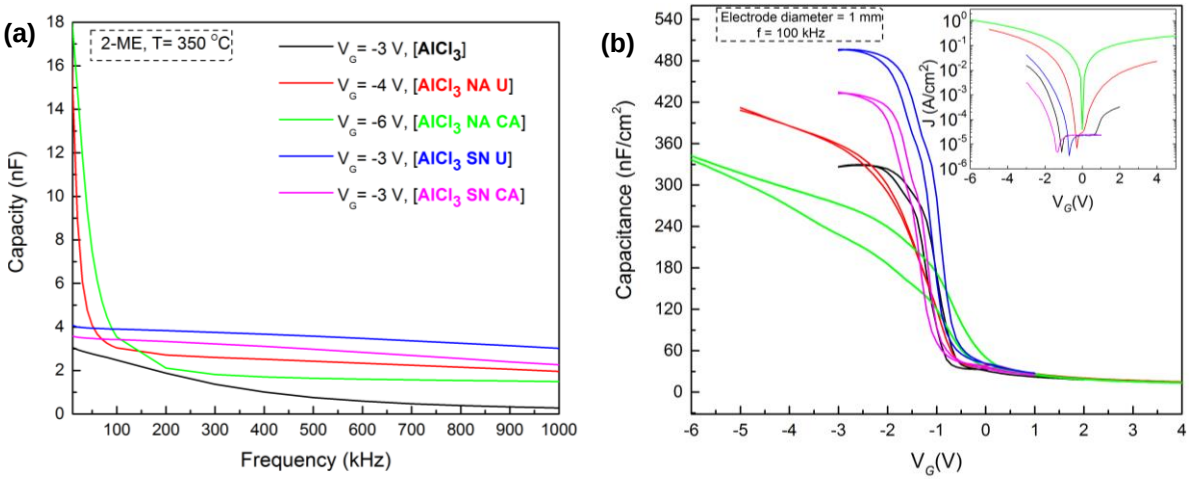

Figure 6.10 – a) Capacity-frequency and b) Capacitance−voltage characteristics with IV curves of p-Si/AlO_x/Al MIS capacitors produced with chloride precursor solution without and with nitrates (ammonium nitrate (NA) or silver nitrate (SN)) using urea (U) or citric acid (CA) as organic fuels in 2-methoxyethanol (2-ME) annealed at 350 ºC over 30 min to a frequency of 100 kHz

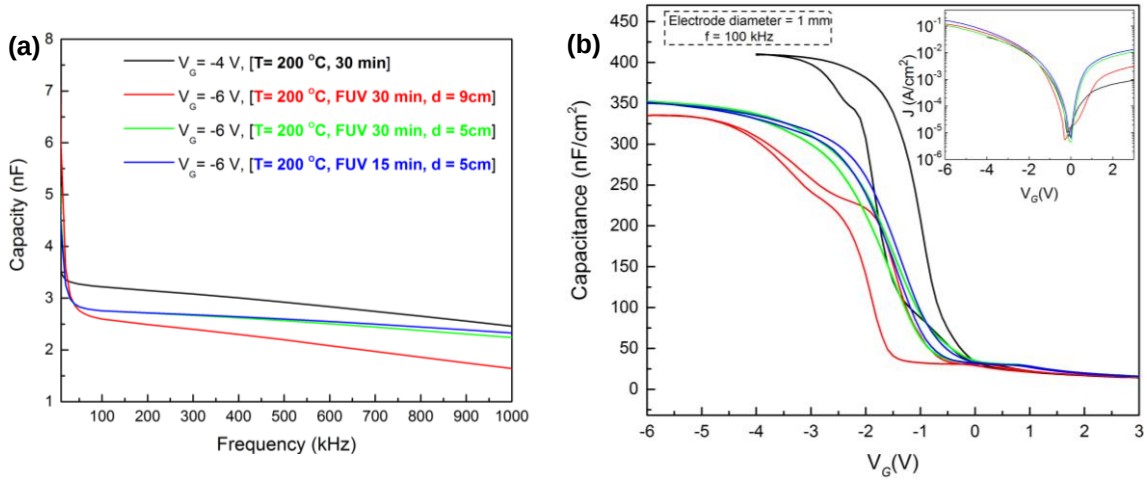

Figure 6.11 – a) Capacity-frequency and b) Capacitance−voltage characteristics with IV curves of p-Si/AlO_x/Al MIS capacitors annealed at 200 ºC without and with FUV irradiation for different times of annealing and lamp distances to a frequency of 100 kHz.

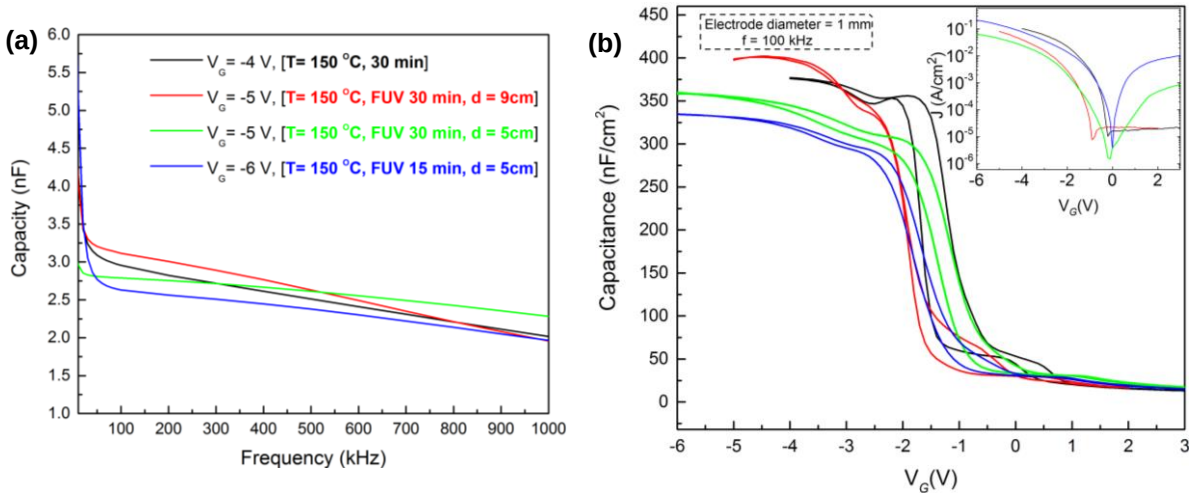

Figure 6.12 – a) Capacity-frequency and b) Capacitance−voltage characteristics with IV curves of p-Si/AlOx/Al MIS capacitors annealed at 150 ºC without and with FUV irradiation for different times of annealing and lamp distances to a frequency of 100 kHz.

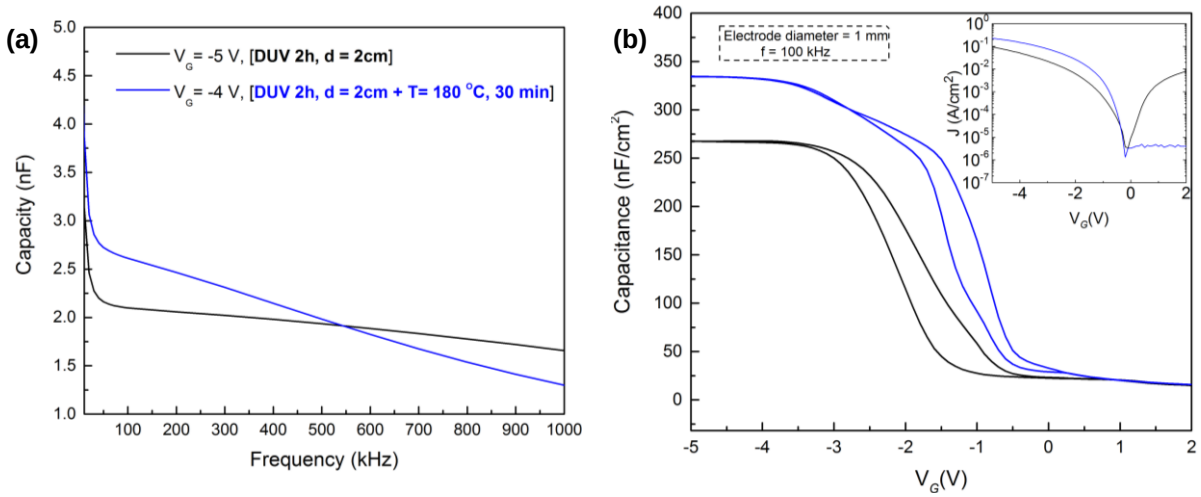

Figure 6.13 – a) Capacity-frequency and b) Capacitance−voltage characteristics with IV curves of p-Si/AlOx/Al MIS capacitors using DUV irradiation for 2 h and after an annealing at 180 ºC for 30 min to a frequency of 100 kHz.

Annex I

Channel dimensions with and without patterning

Table 6.7 – Different sizes of the channels with and without patterning

Channel	**W** (µm)	**L** (µm)	**W/L**
Patterned	200	50	4
Not patterned	600	50	12
Patterned	200	200	1
Not patterned	600	200	3
Patterned	1000	100	10
Not patterned	1400	100	14
Patterned	1000	200	5
Not patterned	1400	200	7

Annex J

Transfer characteristics of ZTO and GIZO TFTs using aluminum chloride with and without fuel as dielectric precursor solution annealed at 350 ºC

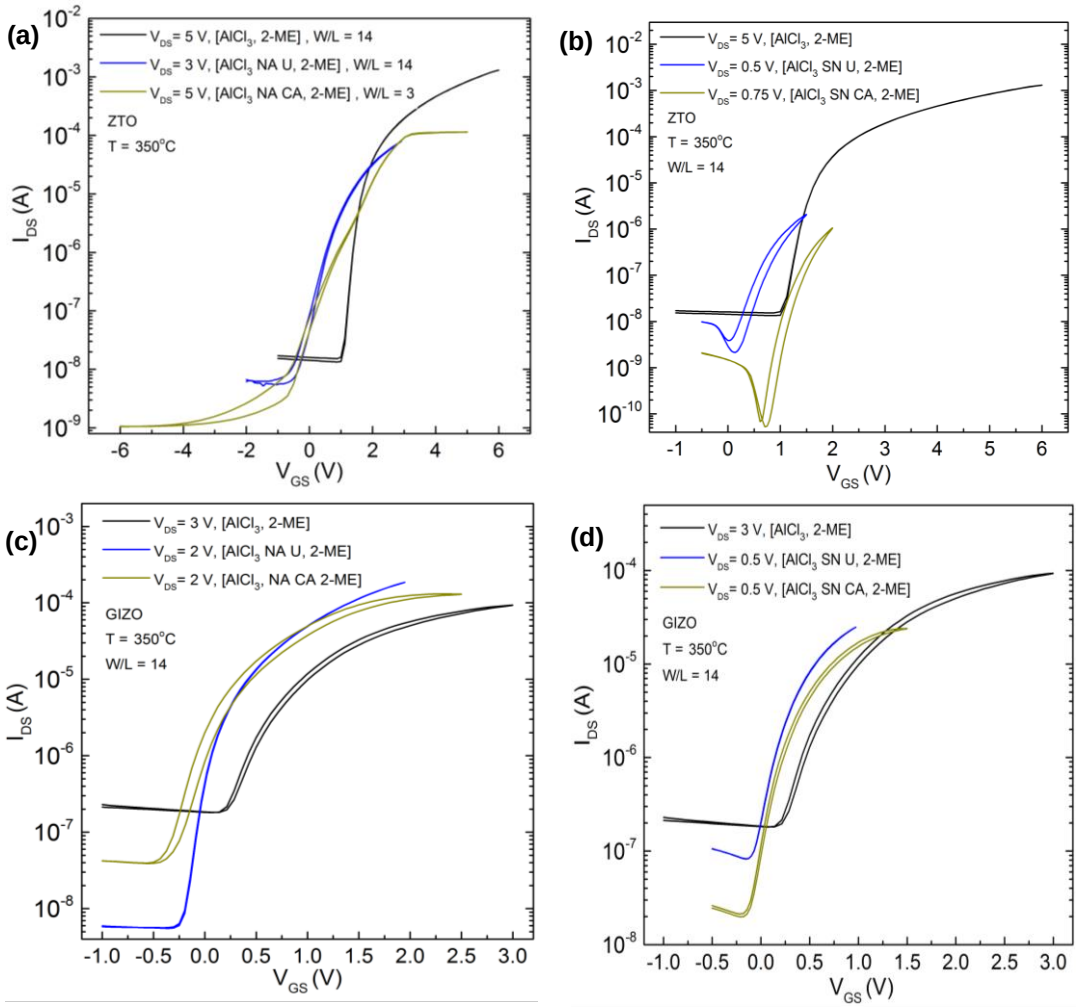

Figure 6.14 – Transfer curves of ZTO TFTs with dielectric of aluminum chloride precursor solution with a) ammonium nitrates (NA) or b) silver nitrates (SN) using urea (U) or citric acid (CA) as fuel in 2-Methoxyethanol, and without at 350 ºC. Transfer curves of GIZO TFTs with dielectric of aluminum chloride precursor solution with c) NA or d) SN using U or CA as fuel in 2-ME, and without at 350 ºC.

Table 6.8 – Electrical properties obtained for the devices depicted in Figure 6.14.

Semiconductor	**Dielectric Solution** ($AlCl_3$)	**T=350 ºC**						
		Von (V)	**I_{ON}/I_{OFF}**	**V_T** (V)	**S** (V/dec)	**μ_{SAT}** (cm^2/Vs)	**V_{Hyst}** (V)	**$I_{G\ max}$** (A)
GIZO sputtering	2-ME	0.14	5.14×10^{2}	0.25	0.30	8.70	0.07	6.09×10^{-4}
	NA U, 2-ME	-0.36	3.36×10^{4}	-0.01	0.11	18.96	0	2.31×10^{-5}
	NA CA, 2-ME	-0.56	3.3×10^{3}	-0.13	0.22	14.54	0.12	9.08×10^{-4}
	SN U, 2-ME	-0.15	3×10^{2}	-0.04	0.19	8.40	0	1.67×10^{-5}
	SN CA, 2-ME	-0.21	1.21×10^{3}	-0.02	0.17	5.69	0.04	2.40×10^{-5}
ZTO solution	2-ME	0.88	9.78×10^{4}	1.20	0.16	33.40	0	9.55×10^{-3}
	NA U, 2-ME	-1.38	1.28×10^{4}	0.40	0.46	4.91	0.18	4.57×10^{-5}
	NA CA, 2-ME	-5.41	1.08×10^{5}	0.78	0.64	65.46	0.20	4.08×10^{-3}
	SN U, 2-ME	0.04	5.41×10^{2}	0.32	0.30	0.53	0.18	3.44×10^{-7}
	SN CA, 2-ME	0.62	1.54×10^{4}	1.05	0.14	0.37	0.16	1.58×10^{-6}

Annex K

Characteristic parameters of 22 devices to study the uniformity and reproducibility of GIZO/ AlO_x TFTs produced at 180 ºC combined with FUV radiation at a lamp distance of 5 cm for 30 min. The W/L used was 10.

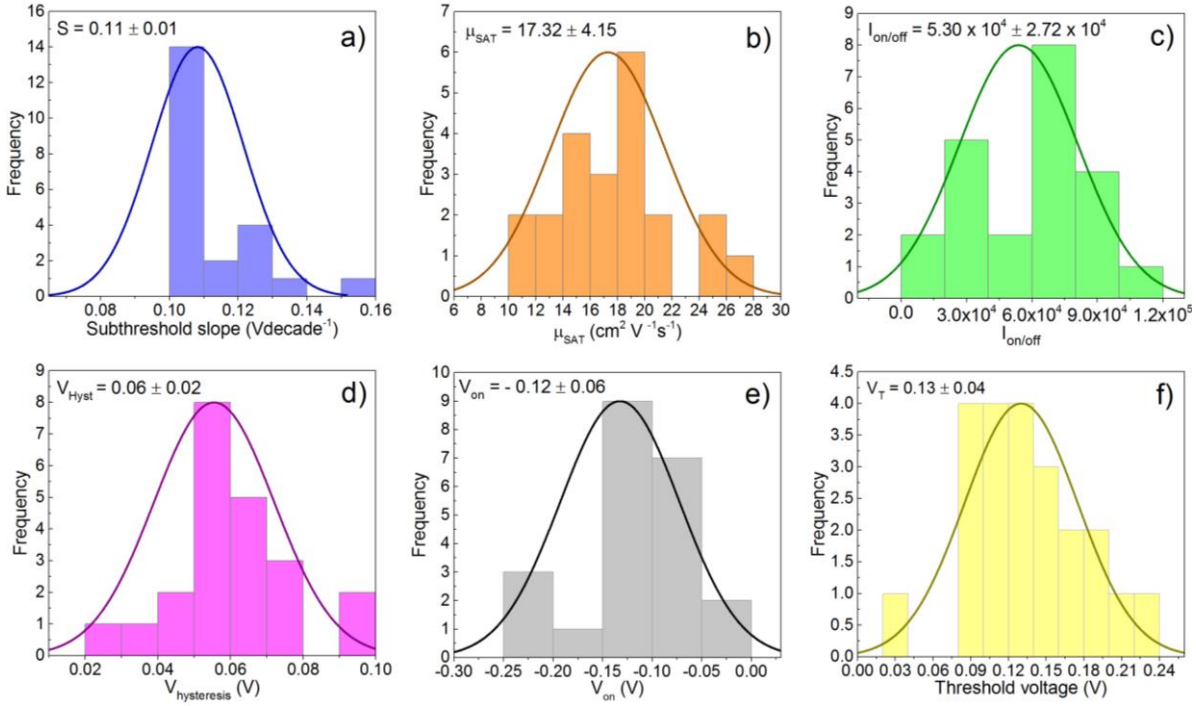

Figure 6.15 – Statistical distributions of a) subthreshold slope (S), b) saturation mobility (μ_{sat}), c) On/Off ratio ($I_{on/off}$), d) hysteresis (V_{Hyst}), e) turn-on voltage (V_{on}) and f) threshold voltage (V_T) for GIZO/ AlO_x TFTs on Si.

Annex L

Stress measurements under a constant V_{GS} in vacuum to study the instability mechanisms on GIZO/ AlO_x TFTs produced at 180 ºC combined with FUV radiation at a lamp distance of 5 cm for 30 min.

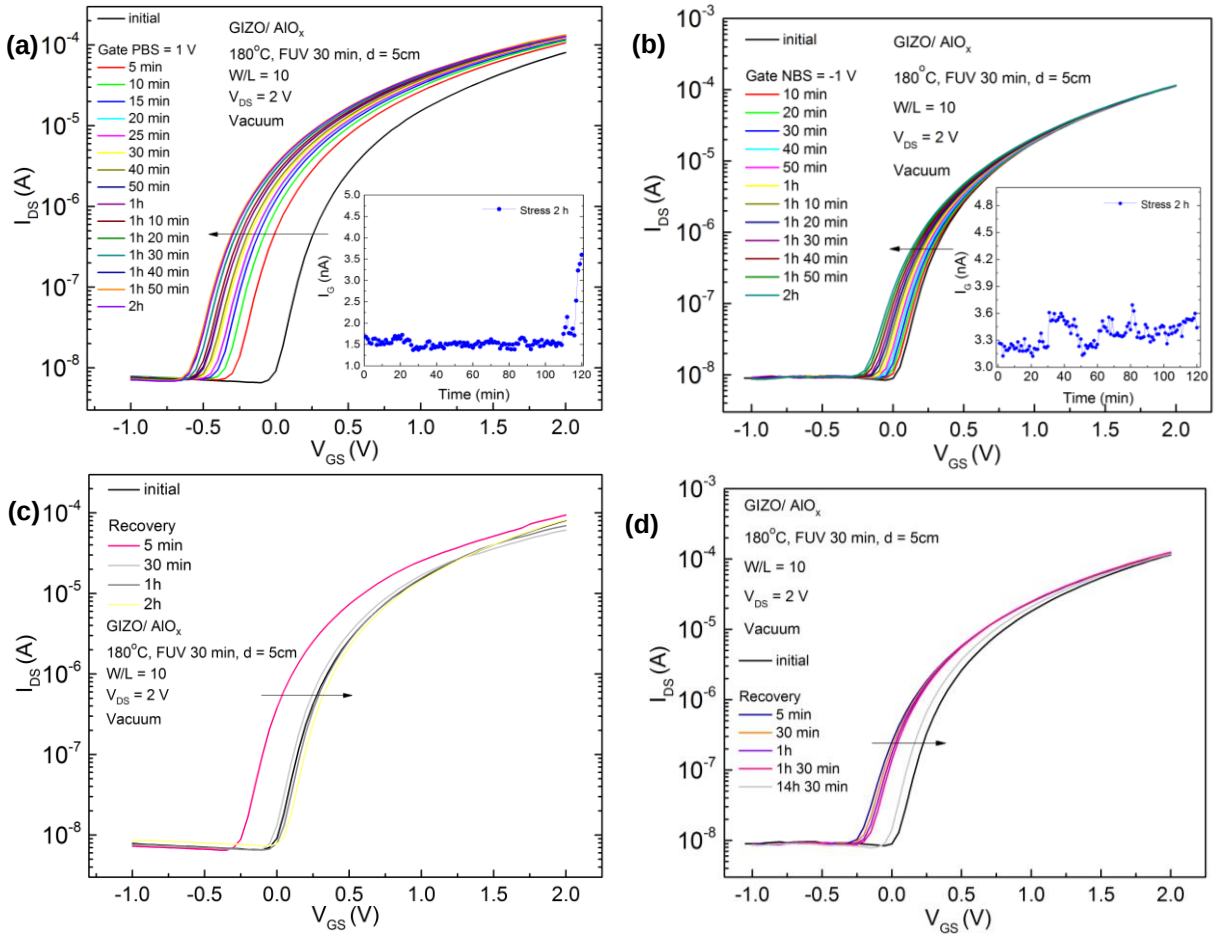

Figure 6.16 – Results obtained for a) a positive gate-bias stress (PBS) and b) a negative gate-bias stress (NBS) stress measurements on GIZO/AlO_x TFTs annealed at 180 ºC with FUV irradiation over 30 min and their recovery, c) and d), respectively.

Annex M

Aging effects on devices produced with the dielectric at 150 ºC combined with FUV radiation at a lamp distance of 5 cm for 30 and 15 min during 9 weeks.

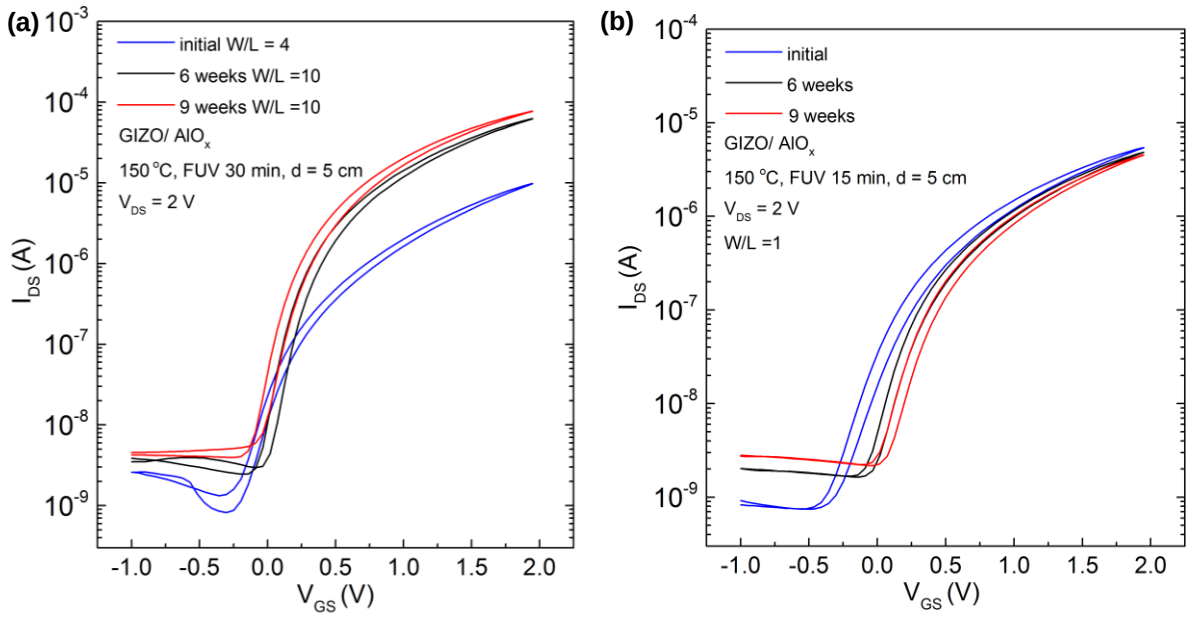

Figure 6.17 – Aging effects seen by the evolution of the transfer characteristics of GIZO/AlO$_x$ TFTs with different dielectric processing conditions: Annealed at 150 ºC with FUV radiation for a) 30 and b) 15 min.

Table 6.9 – Electrical properties obtained for the devices depicted in Figure 6.17

Condition	Time (min)	Measure	$\frac{W}{L}$	Von (V)	I_{ON}/I_{OFF}	V_T (V)	S (V/dec)	μ_{SAT} (cm^2/Vs)	V_{Hyst} (V)
150 ºC + FUV d = 5 cm	30	initial	4	-0.30	1.00×10^4	0.13	0.17	6.66	0.06
		6 weeks	10	-0.09	2.11×10^4	0.16	0.12	14.10	0.07
		9 weeks	10	-0.20	1.70×10^4	0.13	0.13	14.62	0.07
	15	initial	1	-0.52	7.24×10^3	0.03	0.23	11.50	0.09
		6 weeks		-0.14	2.95×10^3	0.13	0.19	10.43	0.07
		9 weeks		-0.04	2.08×10^3	0.18	0.19	10.65	0.07

Annex N

Comparison of our devices fully solution based with literature.

Table 6.10 – Selected processing details for several reported solution based TFTs deposited by spin-coating ("--" means that the related data is not mentioned in the literature).

Ref.	TFT	T (°C)	Time of annealing	S (V dec^{-1})	Mobility (cm^2 V^{-1} s^{-1})	$I_{ON/OFF}$	V_{ON} (V)	V_G range (V)
[1]	In_2O_3/ AlO_x	200	1h 30 min	0.14	12.6	10^4	0.1	- 0.6–2
[69]	In_2O_3/ AlO_x	250	3h 50 min	0.27	82	10^4	- 0.1	- 1–3
[70]	GZTO/ AlO_x	350	2h 30 min	0.30	1.3	10^4	0.5	- 2–5
[71]	ZnO/ (ZrO_2/Al_2O_3-F)	150	33 min	0.08	1.37	10^6	~0	- 0.1–3
[48]	ZTO/ AlO_x	350	4 h	0.25	2.6	10^4	~0	- 1–4
[34]	InO_x/ Al_2O_3	< 150	1 h	--	7.83	10^8	0.2	- 0.5–4
This study	In_2O_3/ AlO_x	200 180	1h 30 min 1h 30 min	0.20 0.15 0.24 0.23	5.57 3.02 1.26 0.55	10^3	~0 0.34 0.23 0.18	- 1–2